Dual wave farms for energy production and coastal protection

J. Abanades[1,2], javier.abanadestercero@plymouth.ac.uk

G. Flor-Blanco[3], gfb@geol.uniovi.es

G. Flor[3], gflor@geol.uniovi.es

G. Iglesias[1*], gregorio.iglesias@plymouth.ac.uk

[1] University of Plymouth, School of Engineering, Marine Building, Drake Circus, Plymouth PL4 8AA, UK

[2] TYPSA Group, Renewable Energy Division, Edificio Manuel Borso, C/ Botiguers, 5 - 5ª planta, 46980 Valencia, Spain

[3] University of Oviedo, Department of Geology, Campus de Llamanquique, C/ Jesus Arias de Velasco, s/n, 33005, Oviedo, Spain

*Corresponding author; e-mail: gregorio.iglesias@plymouth.ac.uk ; tel.: +44.(0)1752 586131.

Dual wave farms for energy production and coastal protection

Abstract

The synergetic application of wave farms, i.e., arrays of wave energy converters (WECs), for protecting the coast in addition to their main objective of generating carbon-free energy can place this renewable resource as a major element in ocean and coastal management. In particular, their ability to mitigate coastal erosion by reducing the amount of wave power reaching the coast will be put to use – and this is the motivation for this work. We propose a new approach in which the wave farm has a dual purpose: to generate carbon-free energy and to contribute to coastal erosion management. We illustrate this approach by means of a case study: a dual-purpose wave farm off Xago, a beach-dune system in Asturias (N Spain) subject to severe erosion – manifested dramatically in the retreat of the dune – and located in the area earmarked for the first wave farm in Spain. The objective of this work is to establish whether or not the wave farm may be useful to counter the erosion of the beach-dune system. To this end a wave propagation model is coupled with a state-of-the-art coastal processes model and applied to analyse the response of the system under storm conditions in two scenarios: with and without the farm. The efficiency of the wave farm in mitigating erosion is determined by comparing the results in both scenarios by means of a series of coastal indicators defined *ad hoc*. We find that the farm reduces storm-induced erosion particularly where it is most acute, in the dune front, and thus contributes to alleviate the current erosive trends. This opens up exciting possibilities of using dual wave farms in lieu of, or as a complement to, coastal structures or beach nourishment. As wave energy develops into a major renewable energy source in the coming decades, dual wave farms are poised to constitute a breakthrough in coastal erosion management.

Keywords: wave energy; coastal management; coastal erosion; beach morphology; sediment transport.

27 ## 1. INTRODUCTION

28 The current status of wave energy is similar to that of wind energy in the early 80's. With a vast
29 resource and a very active R&D community, wave energy is expected to become a major renewable in
30 the coming decades, with wave farms deployed in a number of coastal regions throughout the world
31 (Bernhoff et al., 2006; Cornett, 2008; Folley and Whittaker, 2009; Guedes Soares et al., 2014; Iglesias
32 and Carballo, 2009, 2010b; Pontes et al., 1998; Veigas and Iglesias, 2013, 2014; Vicinanza et al.,
33 2013). In previous work it was established that the extraction of wave energy by a nearshore wave
34 farm results in a milder wave climate in its lee (Carballo and Iglesias, 2013; Iglesias and Carballo,
35 2014; Mendoza et al., 2014; Millar et al., 2007; Palha et al., 2010; Ruol et al., 2011; Smith et al.,
36 2012; Veigas et al., 2014a; Veigas et al., 2014b; Vidal et al., 2007; Zanuttigh and Angelelli, 2013).
37 The scientific hypothesis of this work is that this reduction in wave energy can be used for coastal
38 erosion management, in particular in the case of a beach-dune system. To test the hypothesis, a case
39 study is carried out on Xago Beach, in the area proposed by FAEN (*Fundación Asturiana de la*
40 *Energía*, Asturian Energy Foundation) for the deployment of the first wave farm in Spain. Previous
41 studies of relevance for this work include the characterisation of the wave resource in the region
42 (Iglesias and Carballo, 2010a) and the geological and geotechnical study for wave farm development
43 (Flor-Blanco et al., 2011), in which two areas off the beaches of Xago and Llumeres (Figure 1) were
44 recommended.

45 The Xago beach-dune system constitutes an ideal case study, for it has experienced significant erosion
46 in recent years. This is revealed particularly by the dune toe, which receded up to 11.5 m over a
47 relatively short period of time, 2011-2014 (Figure 2) (Flor-Blanco et al., 2013; Flor et al., 2015). The
48 conventional approach to defending the coast against flooding and erosion involves coastal structures:
49 stone-armour or concrete-unit revetments, seawalls, groynes, detached breakwaters, etc. – this is the
50 so-called "hard engineering" approach. The downsides of this approach are well known: it results in
51 armoured coastlines, which bear little resemblance to their natural counterparts. Structures such as
52 seawalls tend to have high wave reflection coefficients (far higher than those of beaches), which

53 implies larger wave heights in front of the structure and often loss of sediment. Moreover, in the
54 current context of climate change and transition coasts, the inability of structures to adapt to sea-level
55 rise poses a problem. Indeed, there have been recently many cases of coastal structures failing to cope
56 with the increased pressures of climate change (Castelle et al., 2015; Kendon and McCarthy, 2015;
57 Senechal et al., 2015). These examples of failures of coastal structures – due to either structural
58 collapse or excessive overtopping – expose the dramatic consequences of the inadequacy of many of
59 the existing structures in the current transition scenario. The conventional approach to solving this
60 problem entails upgrading the existing structures or building new ones, in both cases at a large cost.

61 On these grounds, nearshore wave farms present three main advantages relative to conventional
62 coastal structures. First, by providing renewable, carbon-free energy, wave farms contribute to
63 decarbonising the energy supply and thereby combatting the manmade causes of climate change.
64 Second, the environmental impact of wave farms on the littoral – the single most sensitive
65 environment in the planet – is considerably lower than that of coastal structures. Last, but not least,
66 wave farms consisting of floating wave energy converters (WECs) – e.g., WaveCat, WaveDragon,
67 DEXA – adapt naturally to sea level rise, and therefore can cope well with the main impact on the
68 littoral of climate change.

69 Thus, rather than resorting to the conventional approach (more structures) to fix obsolete,
70 underperforming structures, deploying wave farms to generate carbon-free energy as their main
71 purpose and, in synergy with it, defend the coastline against erosion and flooding is a new alternative
72 that warrants consideration. Incidentally, their application to coastal defence would enhance the
73 economic viability of wave energy through the savings achieved in conventional defence schemes.

74

75 ## 2. MATERIALS AND METHODS

76 ### 2.1 STUDY SITE

77 Xago (Figure 2) is a ~2 km sandy beach with a flat intertidal area. The sedimentology is characterised
78 by siliciclastic sands of medium size. Their grain size distribution – a prerequisite for the coastal
79 processes model – was established based on sediment samples, and the values of the most relevant
80 metrics (D50 and D90, which are the intercepts for 10%, 50% and 90% of the cumulative mass) were
81 obtained by means of the GRADISTAT model (Blott and Pye, 2001). The tidal regime is semidiurnal,
82 with maximum and mean tidal ranges of 4.98 m and 2.66 m, respectively (Flor-Blanco et al., 2013) –
83 a macro-tidal system close to the transition to meso-tidal. The beach is exposed primarily to waves
84 from the IV quadrant (NW).

85

86 ## 2.2 WAVE PROPAGATION MODEL

87 SWAN (Simulating WAves Nearshore) is a third-generation spectral wave model that solves the
88 equation of conservation of wave action considering the relevant wave generation and dissipation
89 processes, such as shoaling, refraction due to current and depth, whitecapping, bottom friction and
90 depth-induced wave breaking. The deep water boundary conditions were obtained from WaveWatch
91 III (WWIII), a third-generation offshore wave model consisting of global and regional nested grids
92 with a resolution of 100 km (Tolman, 2002). The model was validated over a twelve-month period
93 using data from the wave buoy off Salinas Beach (~1 km to the west of Xago Beach) in conjunction
94 with data from node #3085039 of the SIMAR-44 dataset (off Xago Beach), kindly provided by
95 Spain's State Ports (*Puertos del Estado*).

96 In the twelve-month period considered for model validation purposes (January 2010 - December
97 2010), the average values of significant wave height (H_s), mean period (T_m) and wave direction (θ)
98 were: 1.40 m, 6.02 s and 317.1°, respectively. Storm waves are also typically from the NW; for
99 instance, during the storm from 7th November 2010 to 16th November 2010 the average deepwater
100 wave conditions were: H_s = 3.72 m, T_m = 7.49 s and θ = 299.9°. This period was selected for the
101 assessment of the effects of the wave farm as it presents storm clustering, one of the most relevant

phenomena in coastal erosion (Dissanayake et al., 2015). Indeed, in this period up to four storm peaks occur within approximately a week.

Deepwater wave data from the nearby Avilés offshore wave buoy and hindcast wave data with a three-hourly frequency, along with tidal data from the port of Gijon (20 km away) with an hourly frequency, were used to force the wave propagation and coastal processes models.

As regards wind conditions, in the twelve-month validation period the highest probability of occurrence (22.4%) corresponded to southerly winds (from 157.5° to 202.5°). More importantly, however, the strongest winds (with wind speeds, u_{10}, exceeding 20 ms^{-1}) were associated with northwesterly directions (from 292.5° to 337.5°). Three-hourly values of wind speed and direction obtained from the Global Forecast System (GFS) weather model were input into the wave propagation model.

High-resolution bathymetric and topographic data, obtained in *ad hoc* surveys, were used as input for the coastal processes and wave propagation numerical models (Figure 3). Importantly, the dataset covered not only the submarine beach but also the subaerial beach, including the dune system, with elevations ranging from –20 m to +15 m (with reference to the Spanish National Geodetic Vertical Datum).

In order to locate the WECs accurately and simulate their effects on the nearshore wave conditions, two computational grids with different resolutions were defined (Figure 5): (i) a coarse grid (50 × 50 m), which extended 25 × 25 km and covered part of the Avilés submarine canyon system (including the Avilés Canyon itself, with water depths over 900 m); and (ii) a high-resolution nested grid (12 × 15 m), which extended 5.4 km offshore and 4.5 km from east to west, covering the area of interest.

For the purposes of the modelling in the present research work, the area selected for the wave farm was situated off Xago Beach, at a water depth of ~30 m (Figure 6). Following previous work (Carballo and Iglesias, 2013), the WECs were laid out with a spacing of 2.2D, where D = 90 m is the distance between the twin bows of an individual WaveCat WEC. Their interaction with the wave field

was modelled based on the wave transmission coefficients obtained in laboratory tests (Fernandez et al., 2012). The results of the wave propagation model provided boundary conditions for the XBeach model grid covering the study area (Figure 5).

2.3 COASTAL PROCESSES MODEL

XBeach is a process-based model that predicts the response of the beach under storm conditions considering wave propagation, sediment transport and seabed updates. Wave propagation takes into account the coastal processes in the nearshore area by means of the time-dependent wave action balance coupled to the roller energy equations and the nonlinear shallow water equations of mass and momentum. Sediment transport is modelled applying the depth-averaged advection diffusion equation on the scale of wave groups based on different equilibrium concentration and the Van Rijn–Van Thiel formulation (Van Thiel de Vries, 2009). The complete description of XBeach is given by Roelvink et al. (2006) or Roelvink et al. (2009). XBeach has been successfully applied to predict storm-induced erosion in sandy beaches (Abanades et al., 2014b; McCall et al., 2010; Pender and Karunarathna, 2013; Villatoro et al., 2014) and gravel beaches (Jamal et al., 2014; McCall et al., 2014; Williams et al., 2012).

The computational grid extended some 1.7 km alongshore and 2 km offshore, from the dune system to water depths of approximately 20 m, with a resolution of 7.5 × 5 m. Spectral wave parameters (wave height, period, direction and spreading) from the SWAN runs were used to prescribe the offshore boundary conditions.

Regarding coastal morphodynamics, the beach may be divided into three main sections: (i) the west section, which experiences significant storm-induced erosion; (ii) the middle section, characterised by some erosion on the dune front and deposition in the intertidal area of materials eroded in the west section; and (iii) the east section, subject to intense erosion of the foredune (Flor-Blanco et al., 2013). It is also noteworthy how the evolution of the foredune front has changed over the last years relative to previous decades: whereas the dune limit advanced from 1970 to 2011 (Figure 4), it retreated from 2011 to 2014 (Figure 2). This change from progradation to recession, which may well be related to the

153 severe winter gales experienced in the 2011-2014 period (Flor-Blanco et al., 2013), would highlight
154 the sensitivity of the system to storm-induced erosion, and thus the interest of mitigating the latter
155 from a coastal management perspective.

156 The response of the Xago beach-dune system to storm conditions was compared in two scenarios,
157 with and without the wave farm, in order to establish the effects of the wave farm on the system and,
158 on these grounds, test the scientific hypothesis of this work.

159

160 ## 2.4 COASTAL INDICATORS

161 Coastal indicators were used to quantify the effects of the wave farm on the beach-dune system, as
162 follows. The effects on the nearshore wave conditions were analysed through Reduction in Significant
163 wave Height (*RSH*) (Abanades et al., 2015), a dimensionless indicator defined as

164 $$RSH(x,y) = H_{s,b}(x,y)^{-1}(H_{s,b}(x,y) - H_{s,f}(x,y)) \ , \quad (2)$$

165 where $H_{s,f}$ and $H_{s,b}$ are the significant wave height with the wave farm and without (baseline),
166 respectively, at a generic point of coordinates (x,y). This indicator shows the reduction of the
167 significant wave weight induced by the wave farm in terms of its magnitude in the baseline scenario.

168 The effects of the wave farm on coastal morphodynamics were studied by means of the coastal
169 indicators developed by Abanades et al. (2014a): (i) Bed Level Impact (*BLI*), (ii) beach Face Eroded
170 Area (*FEA*) and (iii) Non-dimensional Erosion Reduction (*NER*).

171 The *BLI* indicator, with SI units of m, represents the difference in seabed level at a point of the beach
172 between the two scenarios, with and without the farm:

173 $$BLI(x,y) = \zeta_f(x,y) - \zeta_b(x,y), \quad (3)$$

where $\zeta_f(x,y)$ and $\zeta_b(x,y)$ are the seabed level with the farm and without it (baseline), respectively, at a generic point of the beach designated by its coordinates (x,y), and at the point in time considered. The y-axis is directed along the general coastline orientation, with the coordinate increasing towards the eastern end of the beach, and the x-axis is directed along the beach profiles, with the coordinate increasing towards the landward end. A positive or negative value of *BLI* signifies that the presence of the wave farm resulted in a higher (accretion) or lower (erosion) seabed level relative to the baseline (no farm) scenario, respectively.

The *FEA* indicator, with units of m^2, represents the volume of the beach face (the section of the profile exposed to wave uprush) eroded per unit length of beach relative to an initial condition – typically, a point in time before the beginning of the storm considered. It is defined in both scenarios, baseline (FEA_b) and with the wave farm (FEA_f):

$$FEA_b(y) = \int_{x_1}^{x_{\max}} \left[\zeta_0(x,y) - \zeta_b(x,y)\right] dx, \qquad (4)$$

$$FEA_f(y) = \int_{x_1}^{x_{\max}} \left[\zeta_0(x,y) - \zeta_f(x,y)\right] dx, \qquad (5)$$

where $\zeta_0(x,y)$ is the seabed level at the point of coordinates (x,y) at the initial condition (typically, a point in time before the storm), and x_1 and x_{max} are the values of the x-coordinate at the seaward end of the beach face and landward end of the profile, respectively. The *FEA* indicator is a profile function, and hence depends only on the y-coordinate, so it allows the alongside analysis of the erosion in the beach.

Finally, the *NER* indicator is also a profile function, in this case non-dimensional, defined as

$$NER(y) = 1 - \left(x_{\max} - x_1\right)^{-1} \int_{x_1}^{x_{\max}} \left[\zeta_0(x,y) - \zeta_f(x,y)\right]\left[\zeta_0(x,y) - \zeta_b(x,y)\right]^{-1} dx\,. \qquad (6)$$

It expresses the variation in the eroded area of a generic profile (x) caused by the wave farm as a percentage of the total area eroded between the initial condition (typically, a point in time before the

196 storm) and the point in time considered. Thus, a positive or negative value implies a reduction or
197 increase in the eroded area as a result of the wave farm, respectively.

198

199 ## 3. Results and Discussion

200 First, the model was validated using the data from the wave buoy off Avilés (with available data from
201 1st March 2010 – 1st September 2010) and the point SIMAR44-3085039 (1st January 2010 – 1st
202 January 2011). The model results are in excellent agreement with the observations (Figures 7 and 8),
203 as corroborated by the root mean square error and coefficient of determination (Table 1).

204 The effects of the wave farm on beach morphodynamics were analysed by comparing the response of
205 the beach with and without the wave farm to the storm from 7 November 2010, 12:00 UTM to 16
206 November 2010, 06:00 UTM (delimited by dashed lines in Figures 7 and 8). In the significant wave
207 height patterns at 18:00 on 9th November 2010 (Figure 9) an area of wave energy concentration is
208 apparent. During the propagation of waves towards the coast their properties change as a result of
209 their interaction with the seabed (refraction, shoaling, friction). Over an irregular bathymetry (Figure
210 6) this interaction often leads to areas of energy concentration, also known as nearshore hotspots
211 (Iglesias and Carballo, 2010b) – such as the area selected for the deployment of a wave farm off
212 Xago.

213 The effects of the wave farm on wave heights were substantial directly behind the wave farm (Figure
214 9), with a reduction in significant wave height (*RSH*) of over 50%. This reduction decreased towards
215 the coastline due to the energy diffracted from both sides of the farm into its wake; importantly,
216 however, it was still significant near the coastline, with *RSH* values exceeding 15% along the 10 m
217 contour. The farm was not directly in front of the beach but somewhat to the east (Figure 9), which
218 reduced its impact on the conditions in the western part of the beach. This is apparent in the
219 significant wave height values along the 20 m contour (Figure 10) and the resulting *RSH* values
220 (Figure 11). (The 20 m contour itself is depicted in Figure 6). Strictly speaking, *RSH* was non-zero

221 over a 3500 m stretch alongshore. More importantly, however, relevant *RSH* values (above 30%)
222 extended over some 1300 m alongshore – and this, it may be argued, is the alongshore extent of the
223 wave farm wake for practical purposes. Owing to the position of the farm to the east of the beach, the
224 wake extends some distance east of the beach (Figure 11). The maximum *RSH* values within the wake
225 were a hefty ~50%.

226 As regards beach morphodynamics, in the baseline scenario (without the wave farm) the storm
227 produced acute erosion in the subaerial beach, in particular in front of the dune in the eastern part of
228 the beach, with a fall in the beach level of up to 2.5 m (Figure 12). In general, some erosion in front of
229 the dune occurred throughout the beach, in line with the general recessionary trend of the dune toe in
230 the period 2011-14 (Figure 2). The low-tide terrace, for its part, experienced accretion in the west and
231 mid-sections – which would appear to be a consequence of the deposition of the sand eroded from the
232 subaerial beach – and some erosion in the east section of the beach. Further offshore areas with some
233 degree of erosion are interspersed with areas of little erosion.

234 For the analysis of the effects of the wave farm, the coastal indicators defined in Section 2.4 were
235 applied. Based on the *BLI* values after the storm (Figure 13) three main areas can be distinguished: the
236 dune front along the entire beach, the low-tide terrace in the east section, and the low-tide terrace in
237 the west and mid-section of the beach. *BLI* values are positive in the first two areas, negative in the
238 latter. Considering also the results shown in Figure 12, these values indicate that the wave farm
239 reduced storm-induced erosion in the dune front and the east section of the low-tide terrace, and
240 reduced storm-induced accretion in the west and mid-sections of the low-tide terrace.

241 The greatest *BLI* values (over 2 m) were found in the first area, the dune front, and especially in the
242 east section of the beach, which experienced the greatest erosion in the absence of wave farm (Figure
243 12). In the west and middle sections *BLI* values were also significant, between 1-1.5 m. In sum, the
244 wave farm contributed significantly to mitigate storm-induced erosion on the dune front.

245 In the second area, the low-tide terrace in the east section of the beach, the maximum *BLI* values were
246 smaller than those on the dune front but nevertheless relevant – with storm-induced erosion

247 decreasing by up to 1 m over a large area. Thus, in the east section of the beach, both on the dune
248 front and the low-tide terrace, erosion is significantly mitigated, which can be explained by the fact
249 that this area is directly in the lee of the wave farm, with consequential reductions in significant wave
250 heights (*RSH* values of ~50%, Figure 11).

251 Finally, in the third area, the west and middle sections of the low-tide terrace, negative *BLI* values
252 occur. The sediment eroded from other areas is deposited in part here, so the storm actually results in
253 accretion in this area (Figure 12). In this context, the negative values of *BLI* indicate that the wave
254 farm reduces accretion.

255 In sum, the wave farm, by reducing the amount of wave energy that reaches the beach during the
256 storm, dampens the morphodynamics of the system: it reduces both erosion (in the first and second
257 areas) and accretion (in the third area).

258 The wave farm was most effective at countering erosion on the dune front. This is no mean feat given
259 that it was precisely the dune front that experienced the greatest erosion in the baseline scenario.
260 Thanks to the absorption of wave energy by the wave farm the landward reach of erosion was
261 displaced offshore by over 10 m along the three profiles considered, representative of the three
262 sections of the beach (Figure 14): P1 (west), P2 (middle) and P3 (east). In the east section (P3) this
263 displacement reached a very substantial 25 m, which is indicative of the efficiency of the wave farm
264 in mitigating storm-induced erosion in the area directly in its lee.

265 To investigate in particular erosion on the beach face, two coastal indicators were applied: $FEA_b(y)$
266 and $FEA_f(y)$, which represent the area eroded in the beach face at the y profile in the baseline and the
267 wave farm scenarios, respectively (Figure 15). The largest values in both scenarios correspond to the
268 east section of the beach, although significant erosion occurred throughout. The reduction achieved by
269 the wave farm is apparent by comparing the curves of FEA_b and FEA_f, and particularly so in the east
270 section – again, the wave farm is most effective were erosion is most pronounced.

271 Finally, the *NER* indicator represents the reduction in the eroded area caused by the wave farm as a
272 proportion or percentage of the total eroded area in the baseline scenario (Figure 16). The wave farm
273 was found to reduce erosion ($NER > 0$) on most of the beach, with the highest values in the east
274 section ($NER > 60\%$). As indicated, this is precisely the area where the erosion of the beach face was
275 more pronounced in the baseline scenario (Figure 15) – hence the interest for coastal management. In
276 any case, this drastic reduction in erosion in the east section, for all its relevance, must not obscure the
277 significant reductions elsewhere, with an average *NER* value of 17.64%.

278 These results indicate that a wave farm off Xago Beach would have contributed to mitigating the dune
279 erosion over the last decade at the very least during the storm events (short-term analysis). Although
280 further analysis in the long-term would undoubtedly be useful – possibly using behavioural models
281 rather than process-based models – the present results can be of particular relevance in cases with
282 assets (promenades, buildings, roads, railways, etc.) close to the beach and at risk from storm-induced
283 scour at the toe of their foundations, for they indicate that a wave farm deployed off the affected
284 section of coast would contribute to preventing storm-induced toe scour, which may lead to structural
285 failure.

286 However, the effects of wave farms on the coast do not lend themselves to general statements, for
287 they will depend on the characteristics of the area in question (wave energy resource, wave climate
288 and grain size distribution, among others), of the WECs and their layout. In this sense, *ad hoc* studies
289 are necessary for determining the viability of such projects in an area, considering not only the
290 effectiveness of the wave farm in mitigating coastal erosion but also any other effects. In certain
291 cases, these may be negative, e.g. in an coastal area popular with surfers. The reduction in wave
292 power and, consequently, wave height near shore might have a negative impact on the tourism and the
293 economy of the area; in the latter the deployment of the WECs could affect the fisherman's activity
294 and the lower resource could reduce the nutrient flow. On the other hand, in beaches like Xago, that
295 are experiencing a drastic reduction of the sand volume, the installation of a wave farm can contribute
296 for the production of renewable energy and mitigate coastal protection.

297

298 ## 4. CONCLUSIONS

299 This work posited the hypothesis that wave farms can serve for a dual purpose, production of carbon-
300 free energy and coastal erosion management, and tested this hypothesis through a case study: the
301 Xago beach-dune system in N Spain – a beach backed by a dune field which has experienced
302 substantial erosion in recent years, and is located in the area proposed for the deployment of the first
303 wave farm in Spain.

304 To establish the effectiveness of the wave farm in mitigating storm-induced erosion, a series of
305 coastal indicators were applied to the results of two numerical models – a coastal processes model,
306 XBeach, fed by a wave propagation model, SWAN. The wave propagation model was used to
307 determine the effects of the wave farm on the nearshore wave conditions. Wave energy extraction by
308 the WECs was found to have relevant nearshore effects, with reductions in the significant wave height
309 (*RSH*) of up to 50% along the 20 m contour.

310 For the purpose of coastal erosion management the crux of the matter is of course the effects of the
311 wave farm on the morphodynamics of the beach-dune system. These may be summarised as follows:
312 by reducing the amount of wave energy available at the beach, the wave farm acted as a dampener of
313 coastal processes. The areas which experienced erosion under storm conditions (dune front, low-tide
314 terrace in the east part of the beach) saw their erosion mitigated thanks to the wave farm. Similarly,
315 the areas which experienced accretion under storm conditions (low-tide terrace in the west and middle
316 parts of the beach) saw their accretion reduced.

317 Importantly, the farm reduced storm-induced erosion of the dune front. The scarp, or landward
318 extreme reached by erosion, was displaced seaward by up to 25 m in the east part of the beach, i.e. in
319 the section most affected by storm-induced erosion. Had the wave farm been operating, this would
320 have been of great practical significance, given the unrelenting retreat of the dune toe experienced by
321 the beach in the period 2011-14.

322 Further research is certainly warranted to validate our hypothesis, and analysis at the local scale will
323 always be necessary. In any case, the results so far are promising as to the potential of dual-purpose
324 wave farms to serve as a coastal erosion management tool, replacing, or at least complementing,
325 conventional coastal structures (detached breakwaters, groynes, etc.) which tend to have far greater
326 visual impact and, unlike offshore floating wave farms, do not adapt naturally to sea level rise – an
327 important aspect in the current context of climate change.

328 For this new approach to wave energy, the dual-purpose wave farm, to materialise, its benefits in
329 terms of coastal management must be translated into incentives for the developers of the wave farms;
330 in economic terms, the positive externalities (reduced storm-induced erosion, reduced visual impact,
331 etc.) must be internalised through appropriate mechanisms (Astariz and Iglesias, 2015a; Astariz and
332 Iglesias, 2015b; Astariz and Iglesias, 2016). If correctly applied, the potential of this new approach is
333 immense.

334 In sum, with the advent of large scale wave energy exploitation over the coming decades, a new,
335 potent tool for coastal erosion management will arise.

336

337 **AKNOWLEDGEMENTS**

338 This research was carried out in the framework of the Marie Sklodowska Curie Individual Fellowship
339 WAVEIMPACT, Wave Farm Impacts and Design (Marie Curie Fellow, G. Iglesias), funded by the
340 European Commission, PCIG13-GA-2013-618556, and was partly funded by the School of
341 Engineering of the University of Plymouth (UK). The authors are grateful to *Cluster de Energía,*
342 *Medioambiente y Cambio Climático* of Oviedo (Spain) and Spain's State Ports (*Puertos del Estado*)
343 for kindly providing the data.

344

345 **REFERENCES**

Abanades, J., Greaves, D., Iglesias, G., 2014a. Coastal defence through wave farms. Coastal Engineering 91, 299-307.
Abanades, J., Greaves, D., Iglesias, G., 2014b. Wave farm impact on the beach profile: A case study. Coastal Engineering 86, 36-44.
Abanades, J., Greaves, D., Iglesias, G., 2015. Coastal defence using wave farms: The role of farm-to-coast distance. Renewable Energy 75, 572-582.
Astariz, S., Iglesias, G., 2015a. The economics of wave energy: A review. Renewable and Sustainable Energy Reviews 45, 397-408.
Astariz, S., Iglesias, G., 2015b. Enhancing Wave Energy Competitiveness through Co-Located Wind and Wave Energy Farms. A Review on the Shadow Effect. Energies 8, 7344-7366.
Astariz, S., Iglesias, G., 2016. Wave energy vs. other energy sources: A reassessment of the economics. International Journal of Green Energy.
Bernhoff, H., Sjöstedt, E., Leijon, M., 2006. Wave energy resources in sheltered sea areas: A case study of the Baltic Sea. Renewable Energy 31, 2164-2170.
Blott, S.J., Pye, K., 2001. GRADISTAT: a grain size distribution and statistics package for the analysis of unconsolidated sediments. Earth surface processes and Landforms 26, 1237-1248.
Carballo, R., Iglesias, G., 2013. Wave farm impact based on realistic wave-WEC interaction. Energy 51, 216-229.
Castelle, B., Marieu, V., Bujan, S., Splinter, K.D., Robinet, A., Sénéchal, N., Ferreira, S., 2015. Impact of the winter 2013–2014 series of severe Western Europe storms on a double-barred sandy coast: Beach and dune erosion and megacusp embayments. Geomorphology 238, 135-148.
Cornett, A.M., 2008. A global wave energy resource assessment. ISOPE--579
Dissanayake, P., Brown, J., Wisse, P., Karunarathna, H., 2015. Effects of storm clustering on beach/dune evolution. Marine Geology 370, 63-75.
Fernandez, H., Iglesias, G., Carballo, R., Castro, A., Fraguela, J., Taveira-Pinto, F., Sanchez, M., 2012. The new wave energy converter WaveCat: Concept and laboratory tests. Marine Structures 29, 58-70.
Flor-Blanco, G., Flor, G., Pando, L., 2013. Evolution of the Salinas-El Espartal and Xagó beach/dune systems in north-western Spain over recent decades: evidence for responses to natural processes and anthropogenic interventions. Geo-Marine Letters 33, 143-157.
Flor-Blanco, G., Pando, L., García-Quintana, Y., Barranco, A., Suárez, J., Rey, J., Flor, G., 2011. Prospección geológico-geotécnica para la instalación de una estación experimental de energías renovables en la plataforma Off Shore de Asturias.
Flor, G., Flor-Blanco, G., Flores-Soriano, C., 2015. Cambios ambientales por los temporales de invierno de 2014 en la costa asturiana (NO de España). Trabajos de Geología 34.
Folley, M., Whittaker, T., 2009. Analysis of the nearshore wave energy resource. Renewable Energy 34, 1709-1715.
Guedes Soares, C., Bento, A.R., Gonçalves, M., Silva, D., Martinho, P., 2014. Numerical evaluation of the wave energy resource along the Atlantic European coast. Computers & Geosciences 71, 37-49.
Iglesias, G., Carballo, R., 2009. Wave energy potential along the Death Coast (Spain). Energy 34, 1963-1975.
Iglesias, G., Carballo, R., 2010a. Offshore and inshore wave energy assessment: Asturias (N Spain). Energy 35, 1964-1972.
Iglesias, G., Carballo, R., 2010b. Wave energy and nearshore hot spots: The case of the SE Bay of Biscay. Renewable Energy 35, 2490-2500.
Iglesias, G., Carballo, R., 2014. Wave farm impact: The role of farm-to-coast distance. Renewable Energy 69, 375-385.
Jamal, M.H., Simmonds, D.J., Magar, V., 2014. Modelling gravel beach dynamics with XBeach. Coastal Engineering 89, 20-29.
Kendon, M., McCarthy, M., 2015. The UK's wet and stormy winter of 2013/2014. Weather 70, 40-47.

McCall, R.T., Masselink, G., Poate, T.G., Roelvink, J.A., Almeida, L.P., Davidson, M., Russell, P.E., 2014. Modelling storm hydrodynamics on gravel beaches with XBeach-G. Coastal Engineering 91, 231-250.
McCall, R.T., Van Thiel de Vries, J.S.M., Plant, N.G., Van Dongeren, A.R., Roelvink, J.A., Thompson, D.M., Reniers, A.J.H.M., 2010. Two-dimensional time dependent hurricane overwash and erosion modeling at Santa Rosa Island. Coastal Engineering 57, 668-683.
Mendoza, E., Silva, R., Zanuttigh, B., Angelelli, E., Lykke Andersen, T., Martinelli, L., Nørgaard, J.Q.H., Ruol, P., 2014. Beach response to wave energy converter farms acting as coastal defence. Coastal Engineering 87, 97-111.
Millar, D.L., Smith, H.C.M., Reeve, D.E., 2007. Modelling analysis of the sensitivity of shoreline change to a wave farm. Ocean Engineering 34, 884-901.
Palha, A., Mendes, L., Fortes, C.J., Brito-Melo, A., Sarmento, A., 2010. The impact of wave energy farms in the shoreline wave climate: Portuguese pilot zone case study using Pelamis energy wave devices. Renewable Energy 35, 62-77.
Pender, D., Karunarathna, H., 2013. A statistical-process based approach for modelling beach profile variability. Coastal Engineering 81, 19-29.
Pontes, M., Athanassoulis, G., Barstow, S., Bertotti, L., Cavaleri, L., Holmes, B., Mollison, D., Pires, H., 1998. The European wave energy resource, 3rd European Wave Energy Conference, Patras, Greece.
Roelvink, D., Reniers, A., van Dongeren, A., van Thiel de Vries, J., McCall, R., Lescinski, J., 2009. Modelling storm impacts on beaches, dunes and barrier islands. Coastal Engineering 56, 1133-1152.
Roelvink, J., Reniers, A., Van Dongeren, A., Van Thiel de Vries, J., Lescinski, J., McCall, R., 2006. XBeach model description and manual. UNESCO-IHE Institute for Water Education.
Ruol, P., Zanuttigh, B., Martinelli, L., Kofoed, P., Frigaard, P., 2011. Near-shore floating wave energy converters: applications for coastal protection, Proceedings of the international conference of Coastal Engineering 2010, Shanghai.
Senechal, N., Coco, G., Castelle, B., Marieu, V., 2015. Storm impact on the seasonal shoreline dynamics of a meso- to macrotidal open sandy beach (Biscarrosse, France). Geomorphology 228, 448-461.
Smith, H.C.M., Pearce, C., Millar, D.L., 2012. Further analysis of change in nearshore wave climate due to an offshore wave farm: An enhanced case study for the Wave Hub site. Renewable Energy 40, 51-64.
Tolman, H.L., 2002. User manual and system documentation of WAVEWATCH-III version 2.22.
Van Thiel de Vries, J., 2009. Dune erosion during storm surges. Delft University of Technology.
Veigas, M., Iglesias, G., 2013. Wave and offshore wind potential for the island of Tenerife. Energy Conversion and Management 76, 738-745.
Veigas, M., Iglesias, G., 2014. Potentials of a hybrid offshore farm for the island of Fuerteventura. Energy Conversion and Management 86, 300-308.
Veigas, M., López, M., Iglesias, G., 2014a. Assessing the optimal location for a shoreline wave energy converter. Applied Energy 132, 404-411.
Veigas, M., Ramos, V., Iglesias, G., 2014b. A wave farm for an island: Detailed effects on the nearshore wave climate. Energy 69, 801-812.
Vicinanza, D., Contestabile, P., Ferrante, V., 2013. Wave energy potential in the north-west of Sardinia (Italy). Renewable Energy 50, 506-521.
Vidal, C., Méndez Fernando, J., Díaz, G., Legaz, R., 2007. Impact of Santoña WEC installation on the littoral processes. Proceedings of the 7th European wave and tidal energy conference, Porto, Portugal.
Villatoro, M., Silva, R., Méndez, F.J., Zanuttigh, B., Pan, S., Trifonova, E., Losada, I.J., Izaguirre, C., Simmonds, D., Reeve, D.E., Mendoza, E., Martinelli, L., Formentin, S.M., Galiatsatou, P., Eftimova, P., 2014. An approach to assess flooding and erosion risk for open beaches in a changing climate. Coastal Engineering 87, 50-76.

Williams, J.J., de Alegría-Arzaburu, A.R., McCall, R.T., Van Dongeren, A., 2012. Modelling gravel barrier profile response to combined waves and tides using XBeach: Laboratory and field results. Coastal Engineering 63, 62-80.
Zanuttigh, B., Angelelli, E., 2013. Experimental investigation of floating wave energy converters for coastal protection purpose. Coastal Engineering 80, 148-159.

FIGURES

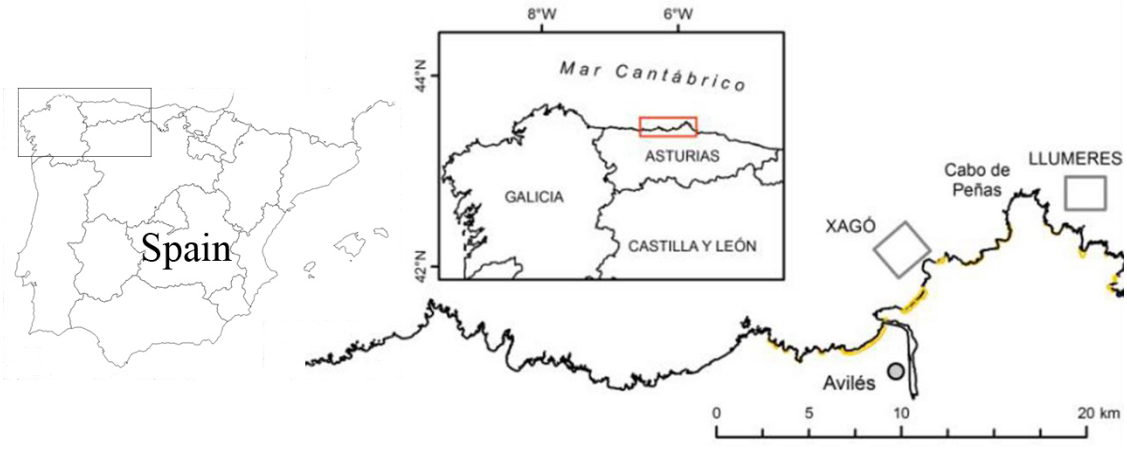

Figure 1: Location of the Xago beach-dune system in Asturias, N Spain. The squares on the right-hand side of the figure delimit the areas selected for the deployment of wave farms: Xago and Llumeres (Flor-Blanco et al., 2011).

458

459 Figure 2: Dune toe recession at Xago.

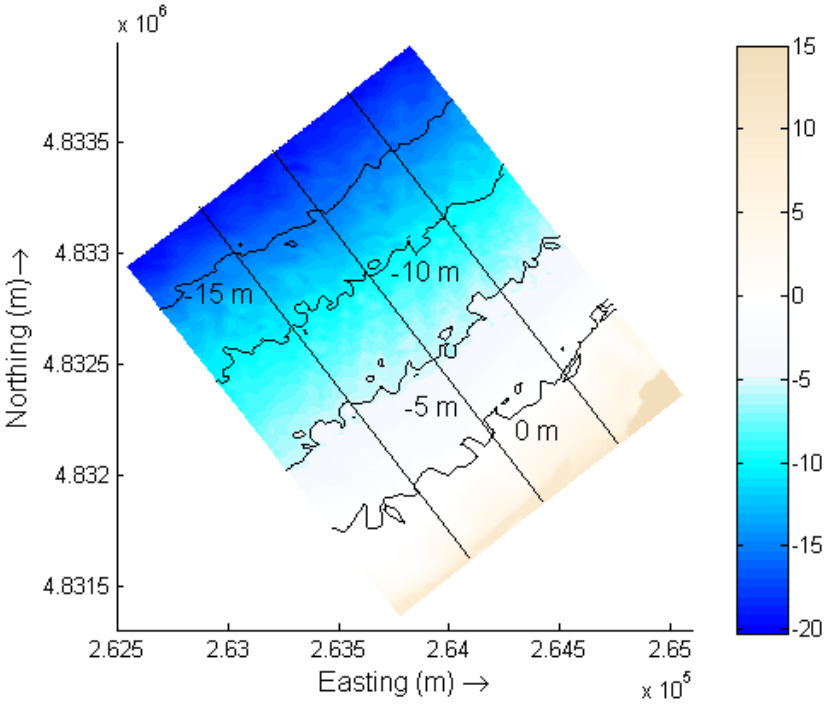

460

461 Figure 3: Bathymetry for the coastal processes model, with Profiles P1, P2 and P3 from left to right.

462 [Water depths in m].

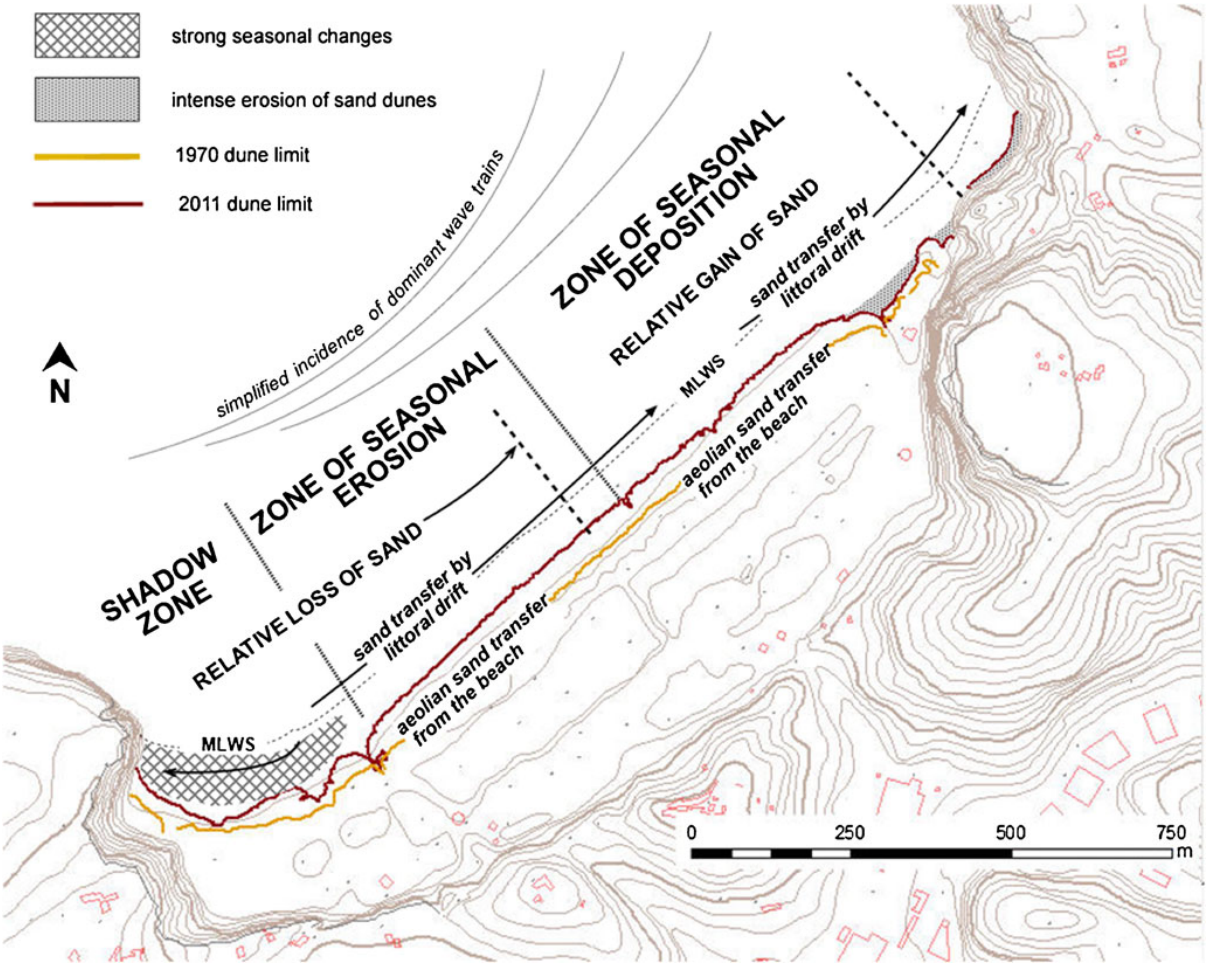

Figure 4: Simplified dynamic and sedimentary model of Xago (Flor-Blanco et al., 2013).

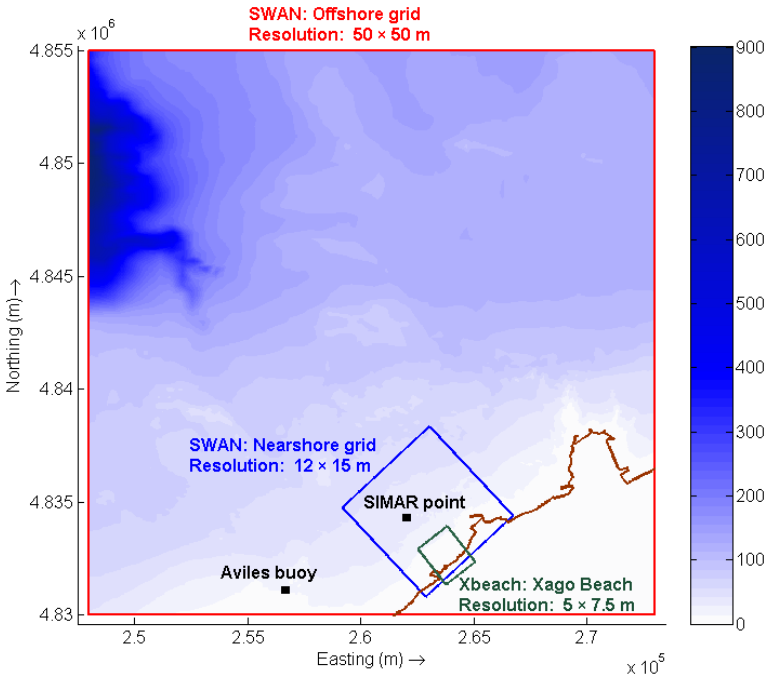

467

468 Figure 5: Computational grids for the SWAN and XBeach models, and wave buoy locations [Water
469 depths in m].

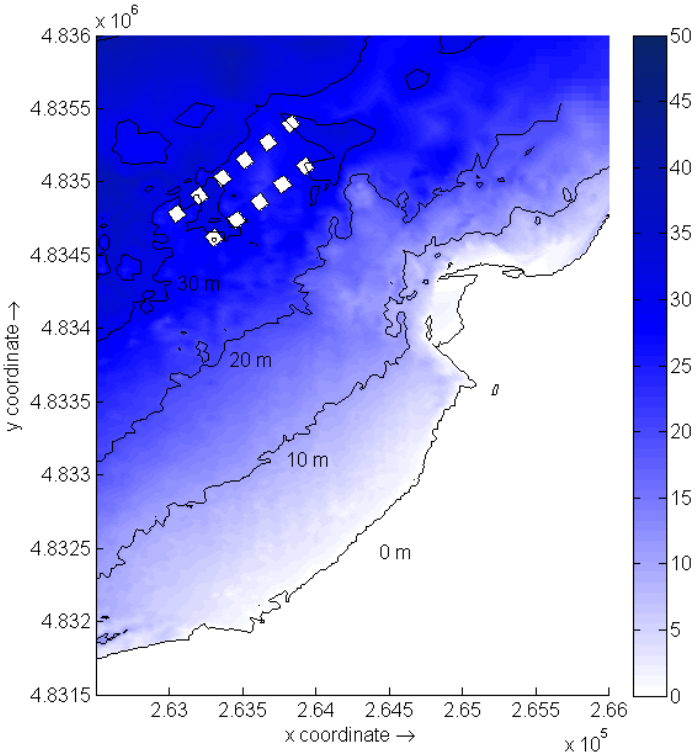

470

471 Figure 6: Wave farm layout off Xago [Water depths in m].

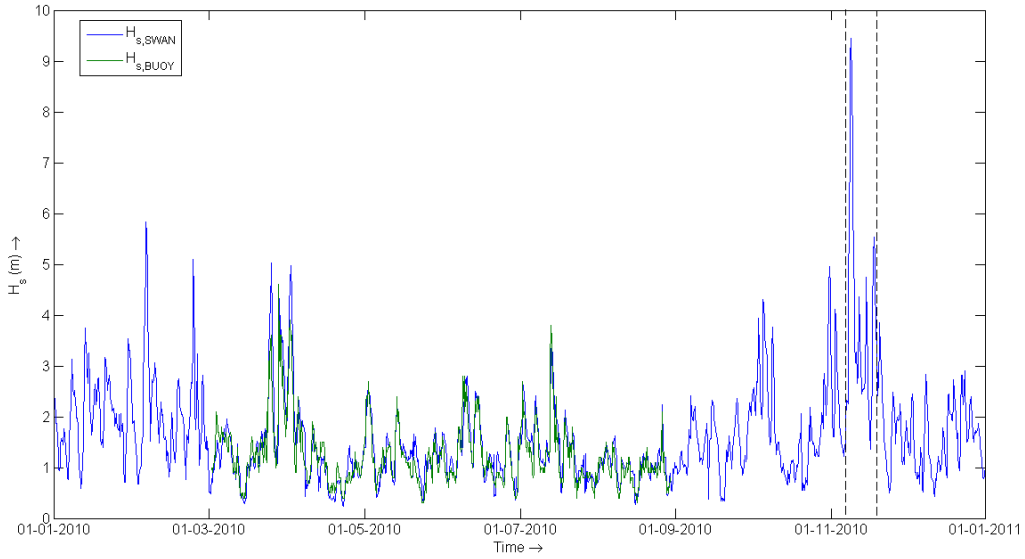

472

473 Figure 7: Validation of the SWAN wave propagation model with the Aviles wave buoy data: observed
474 ($H_{S,\,BUOY}$) *vs.* calculated ($H_{S,\,SWAN}$) time series of significant wave height. The dashed lines delimit the
475 storm period used for the study.

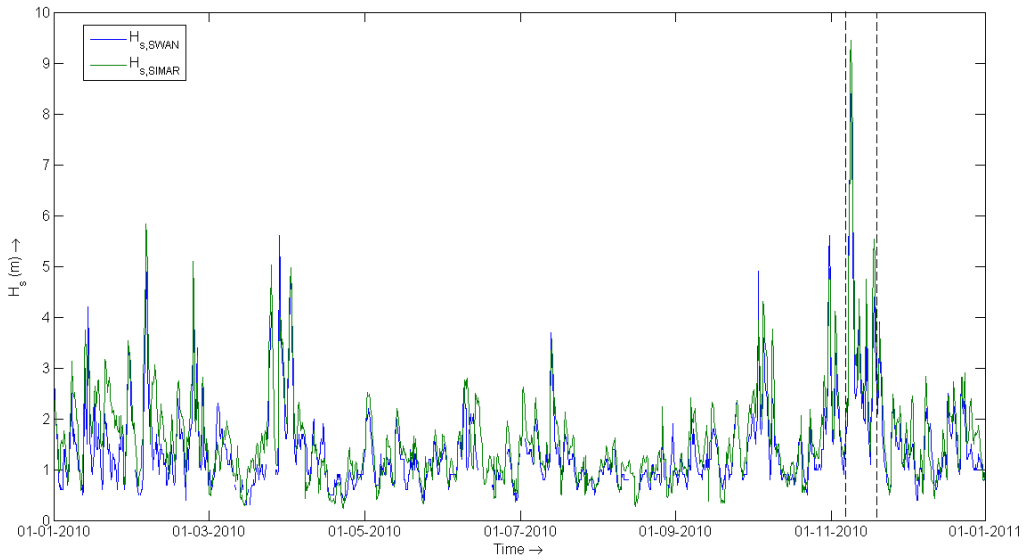

476

477 Figure 8: Validation of the SWAN wave propagation model with the point SIMAR44-3085039 off
478 Xago Beach: observed ($H_{S,\,BUOY}$) *vs.* calculated ($H_{S,\,SWAN}$) time series of significant wave height. The
479 dashed lines delimit the storm period used for the study.

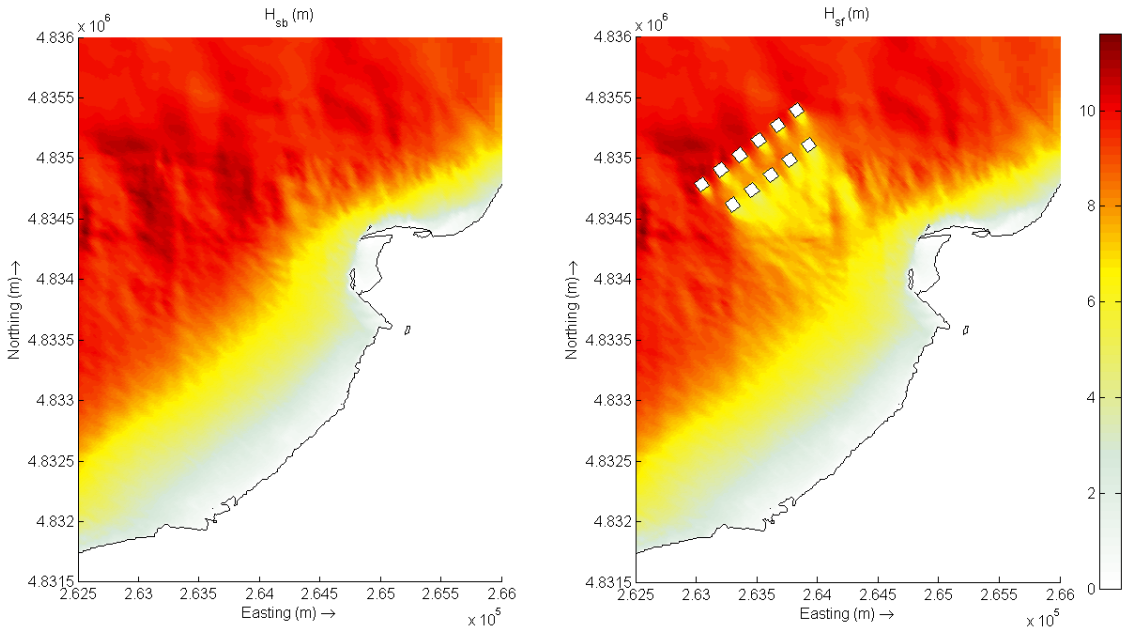

480

481 Figure 9: Significant wave height in the baseline scenario (H_{sb}) and with the wave farm (H_{sf}) on 9 Nov
482 2010, 18:00 UTC. [Deep water wave conditions: H_{s0}=10.28 m, T_p = 15.64 s, θ_p = 268.45°].

483

484

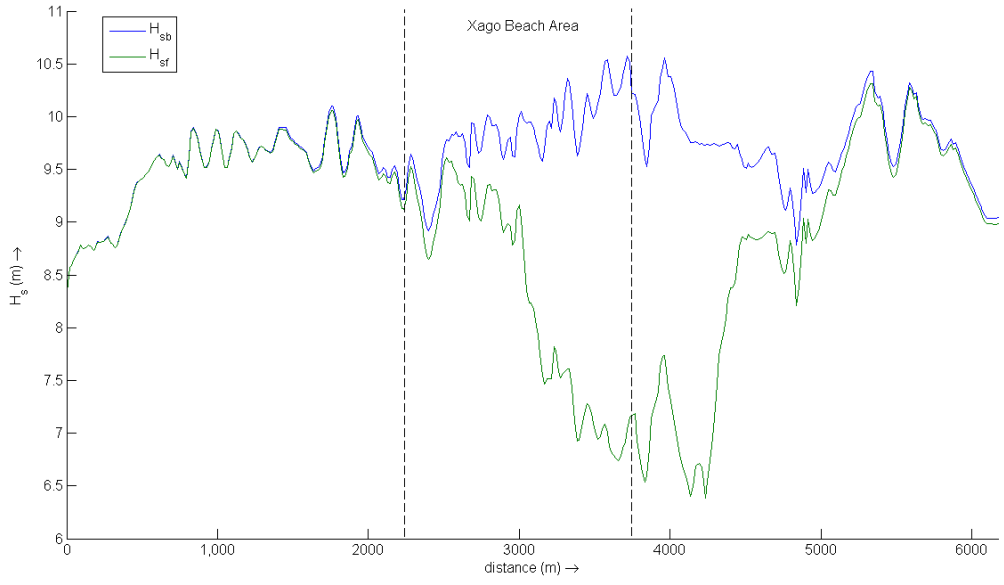

485

486 Figure 10. Significant wave height in the baseline scenario (H_{sb}) and with the wave farm (H_{sf}) along
487 the 20 m water depth contour on 9 Nov 2010, 18:00 UTC. [Deep water wave conditions: H_{s0}=10.28
488 m, T_p = 15.64 s, θ_p = 268.45°].

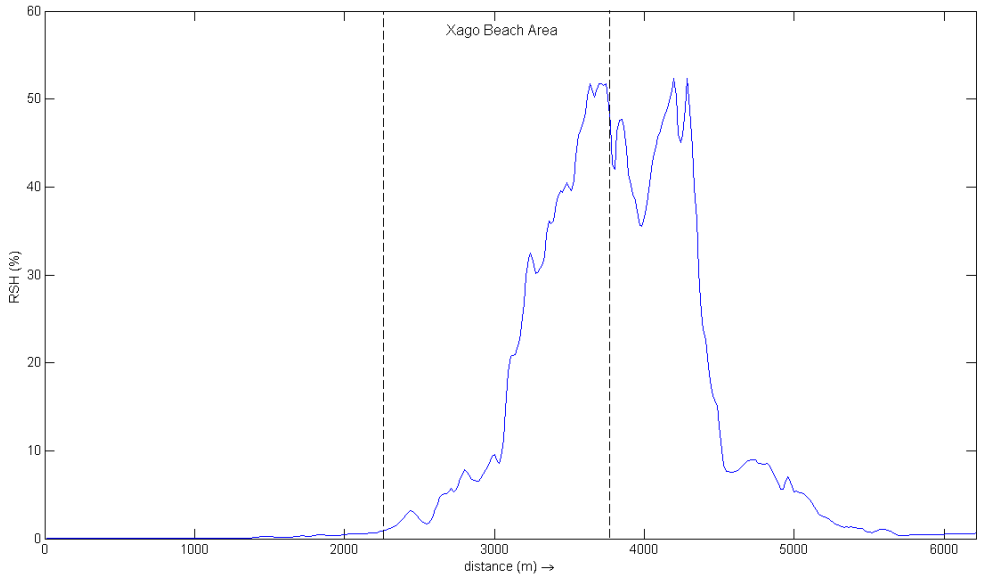

489

490 Figure 11: Reduction of the significant wave height (*RSH*) parameter along the 20 m water depth
491 contour on 9 Nov 2010, 18:00 UTC. [Deep water wave conditions: H_{s0}=10.28 m, T_p = 15.64 s, θ_p =
492 268.45°].

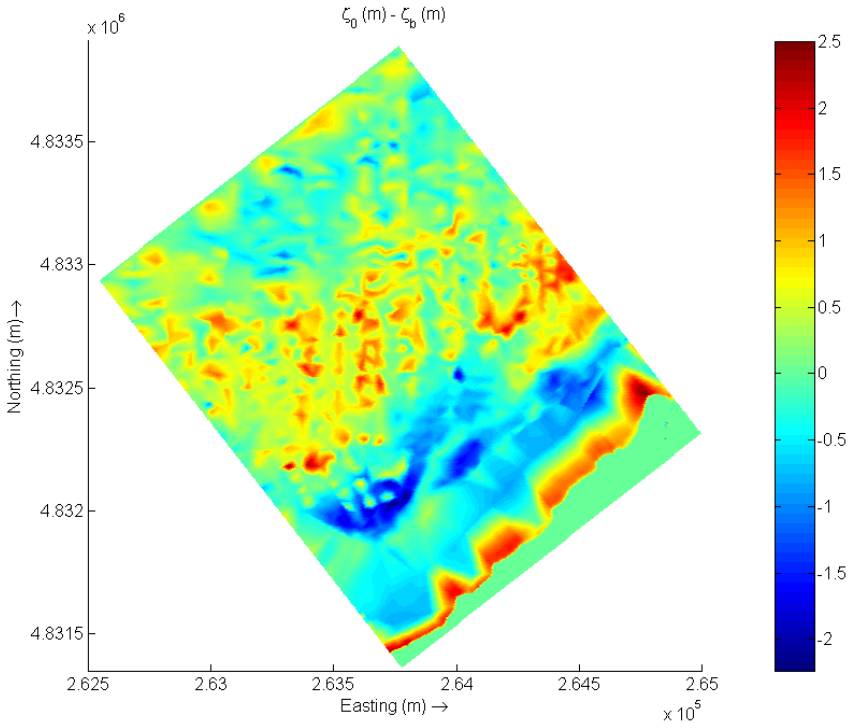

493

494 Figure 12: Fall in bed level after the storm (without the wave farm). Positive and negative values
495 indicate erosion and accretion, respectively.

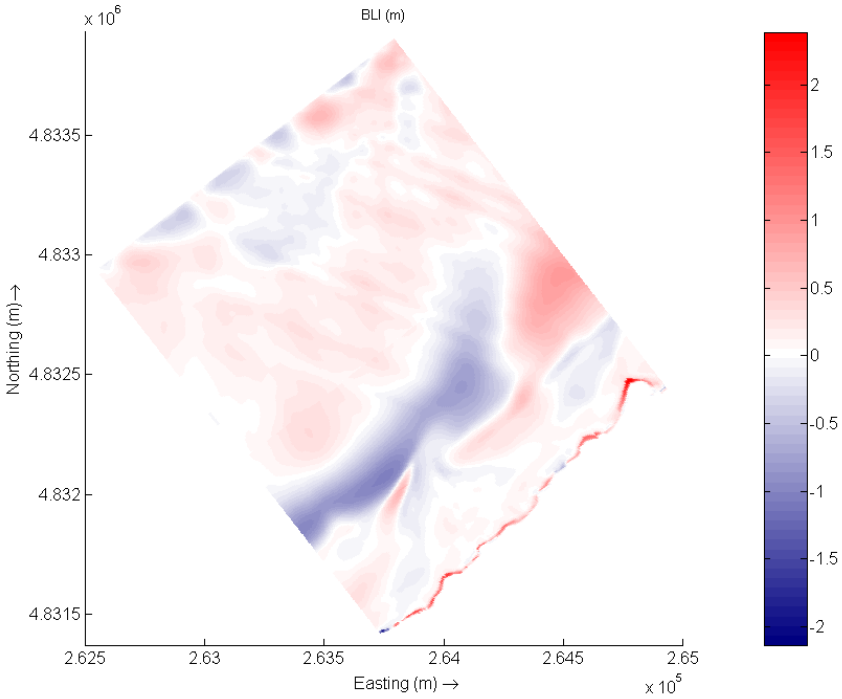

Figure 13: Bed level impact (*BLI*) at Xago after the storm [16 Nov 2007, 06:00 UTC]. Positive values indicate reduction in erosion due to the wave farm.

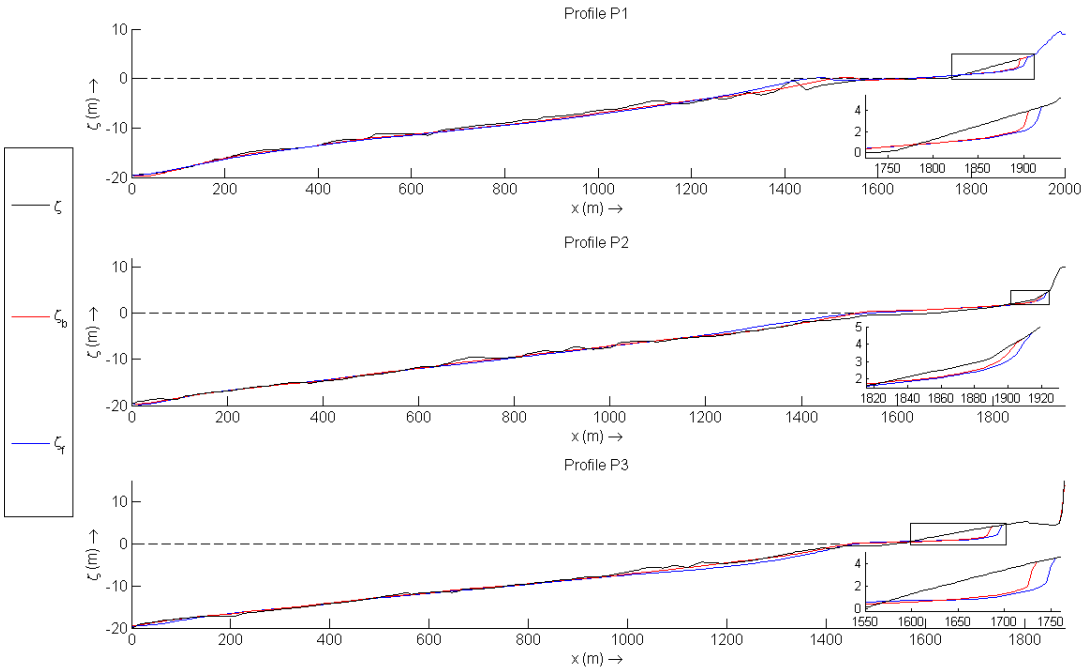

Figure 14: Bed level at profiles P1, P2 and P3: before the storm (ζ_0) [07 Dec 2007, 12:00 UTC] and after the storm [16 Nov 2007, 06:00 UTC] in the baseline scenario (ζ_b) and with the wave farm (ζ_f). [Profiles P1, P2 and P3 are delimited in Figure 3].

508

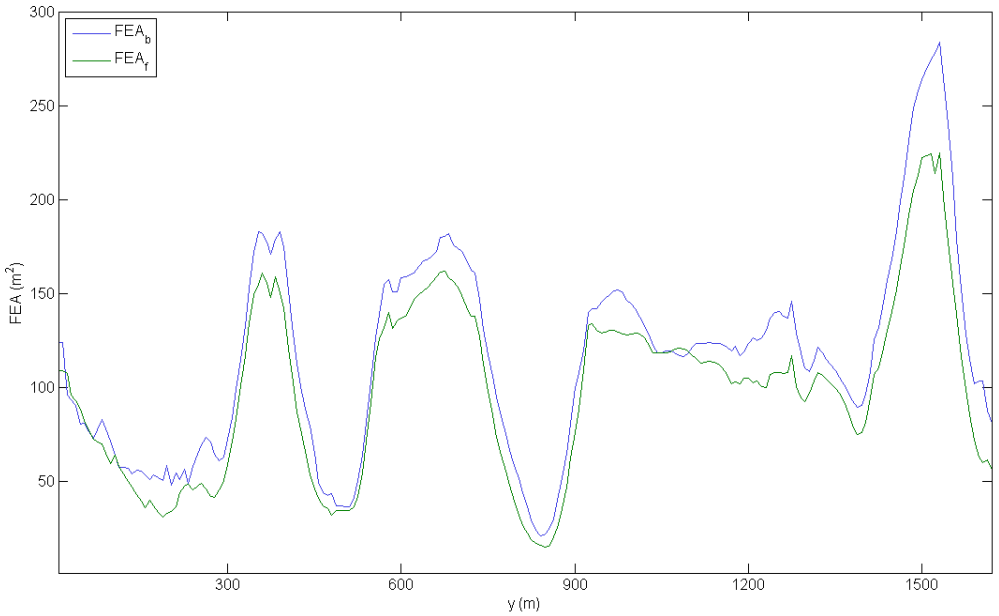

509

510 Figure 15: Beach face eroded area at the end of the time period studied [16 Nov 2007, 06:00 UTC] in
511 two scenarios: baseline (FEA_b) and with the wave farm (FEA_f). The y-coordinate is the alongshore
512 coordinate, with y increasing eastwards.

513

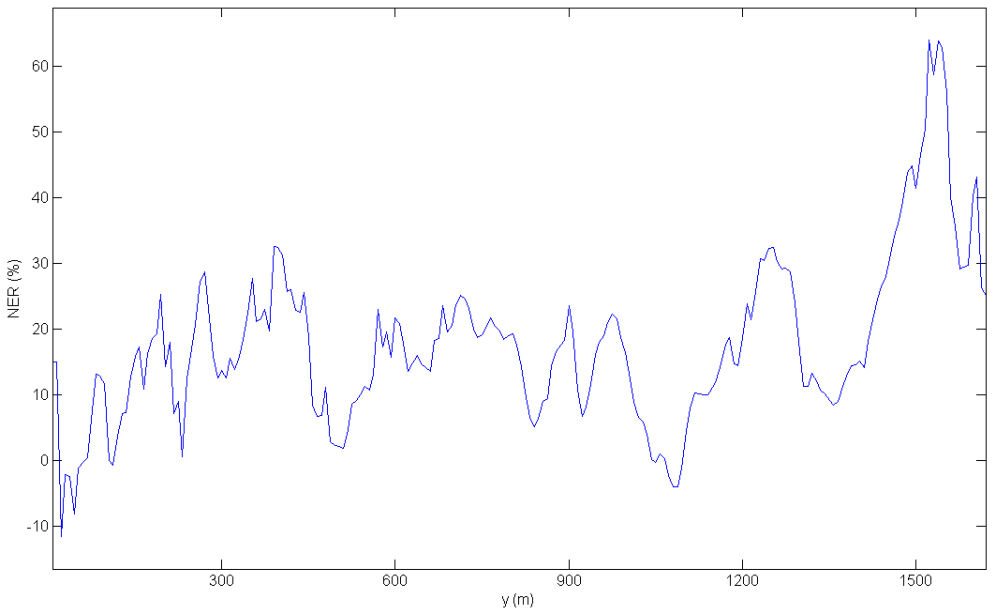

Figure 16: Non-dimensional erosion reduction (NER) on the beach face at the end of the time period studied [16 Nov 2007, 06:00 UTC]. The y-coordinate is the alongshore coordinate, with y increasing eastwards.

520

521 Table 1: Wave data used to validate the wave propagation model and values of the error statistics:
522 Root Mean Square Error (*RMSE*) and coefficient of determination (R^2).

Data	Data available	Error statistics	
		Root Mean Square Error (*RMSE*) [in m]	Coefficient of determination (R^2) [-]
Wave buoy data off Avilés	1st March 2010 – 1st September 2010	0.33	0.89
SIMAR44-3085039 off Xago	1st January 2010 – 1st January 2011	0.45	0.92

523


Legend
2011
2014
N
0
250
500
m

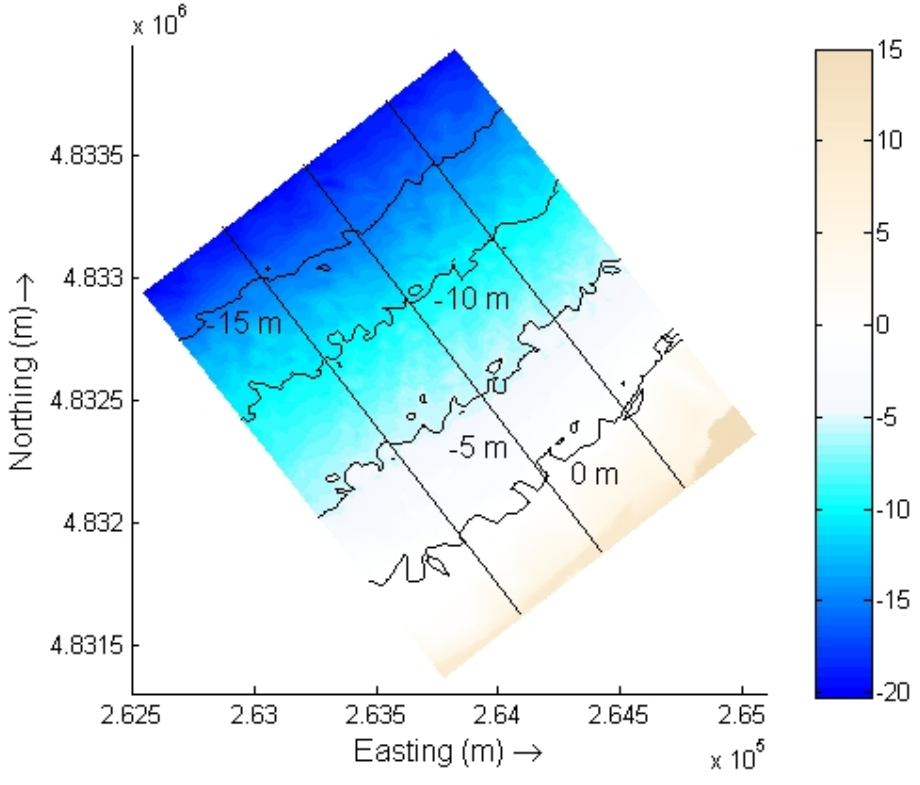
x 10^6
4.8335
4.833
4.8325
4.832
4.8315
Northing (m) →
-15 m
-10 m
-5 m
0 m
2.625
2.63
2.635
2.64
2.645
2.65
Easting (m) →
x 10^5
15
10
5
0
-5
-10
-15
-20

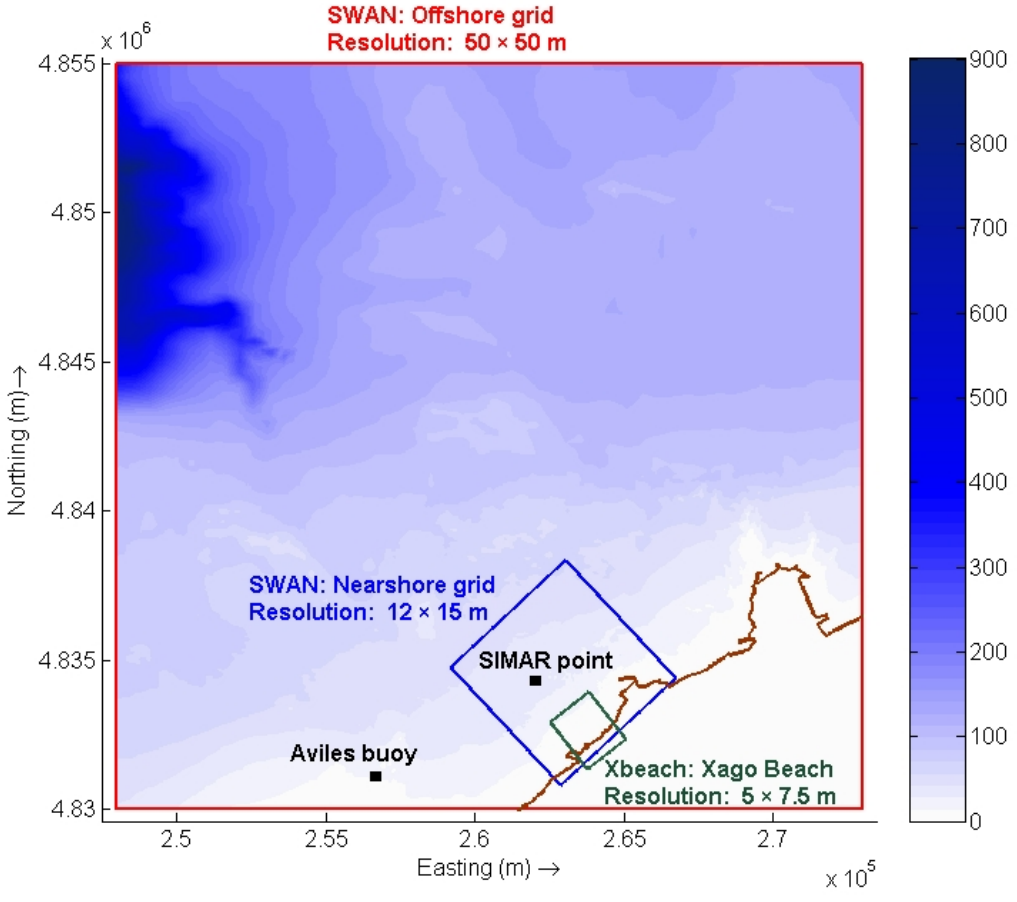
SWAN: Offshore grid
Resolution: 50 × 50 m
x 10^6
4.855
4.85
4.845
4.84
4.835
4.83
Northing (m)→
SWAN: Nearshore grid
Resolution: 12 × 15 m
SIMAR point
Aviles buoy
Xbeach: Xago Beach
Resolution: 5 × 7.5 m
2.5
2.55
2.6
2.65
2.7
Easting (m) →
x 10^5
900
800
700
600
500
400
300
200
100
0

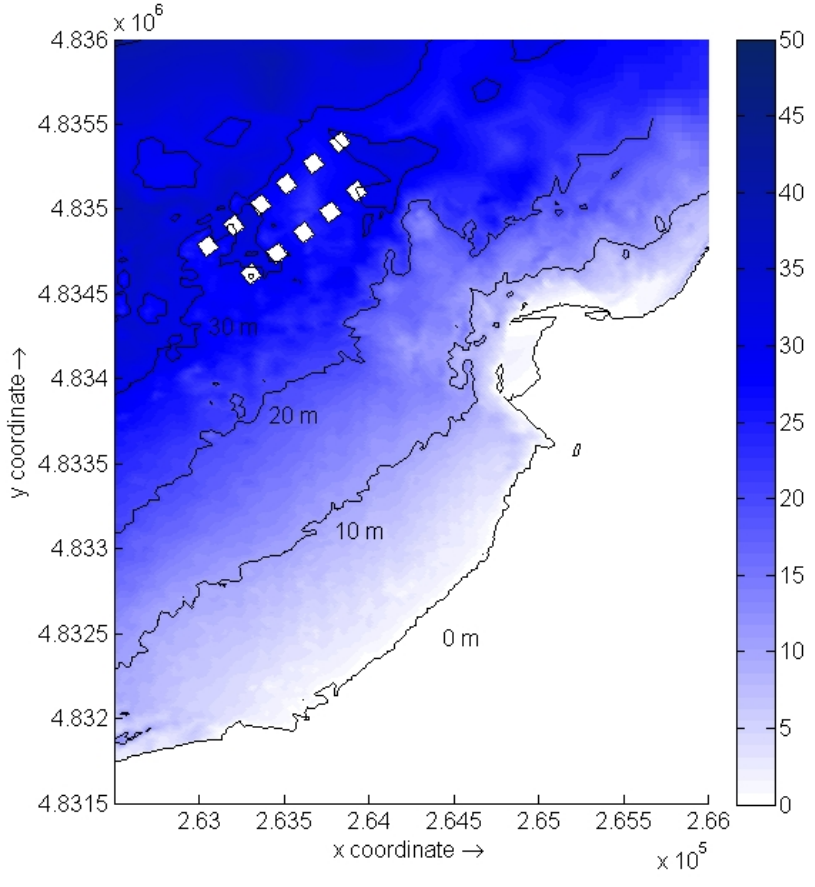
x 10^6
4.836
4.8355
4.835
4.8345
4.834
4.8335
4.833
4.8325
4.832
4.8315
y coordinate →
30 m
20 m
10 m
0 m
2.63
2.635
2.64
2.645
2.65
2.655
2.66
x coordinate →
x 10^5
50
45
40
35
30
25
20
15
10
5
0

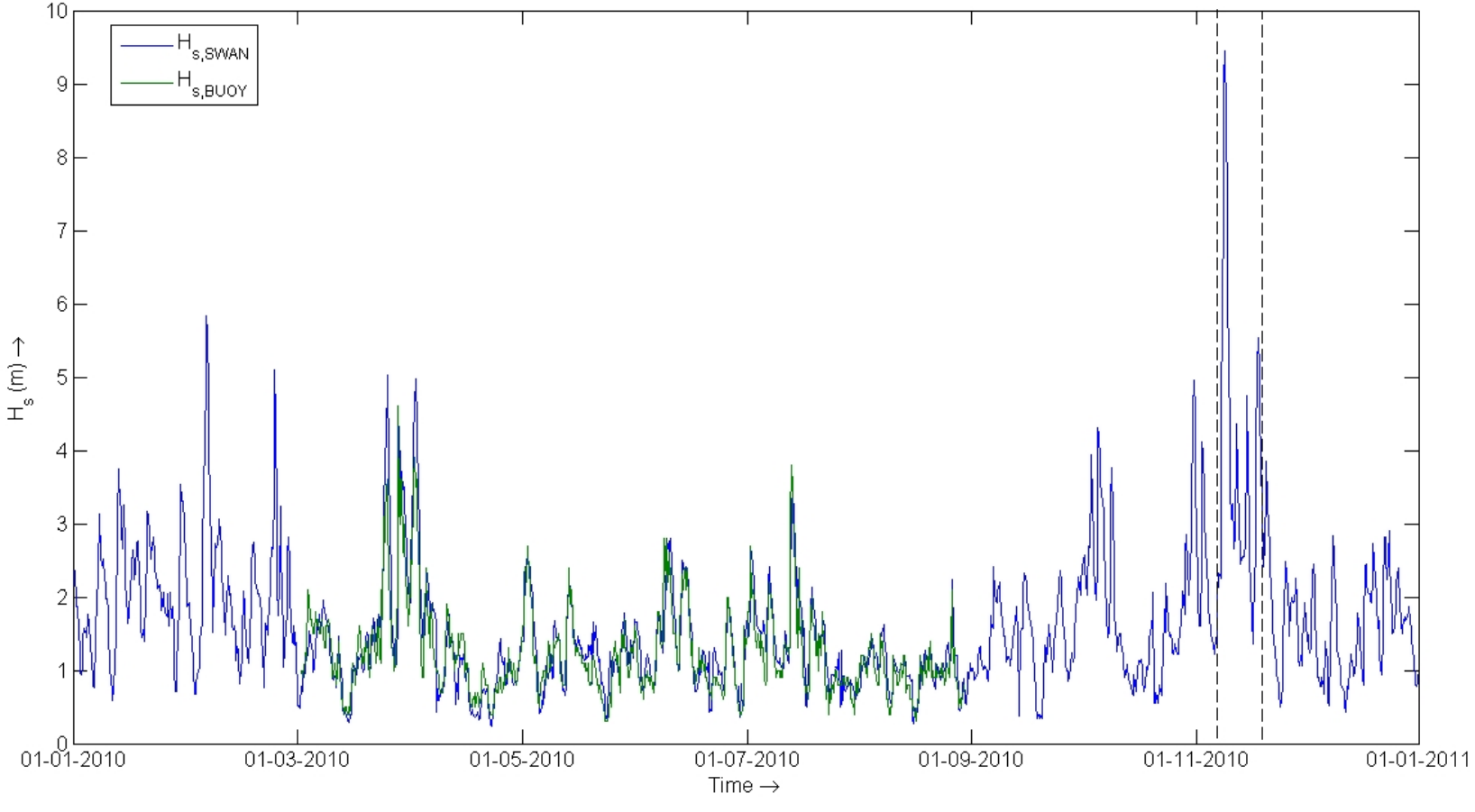
H s,SWAN
H s,BUOY
H s (m) →
Time →
0
1
2
3
4
5
6
7
8
9
10
01-01-2010
01-03-2010
01-05-2010
01-07-2010
01-09-2010
01-11-2010
01-01-2011

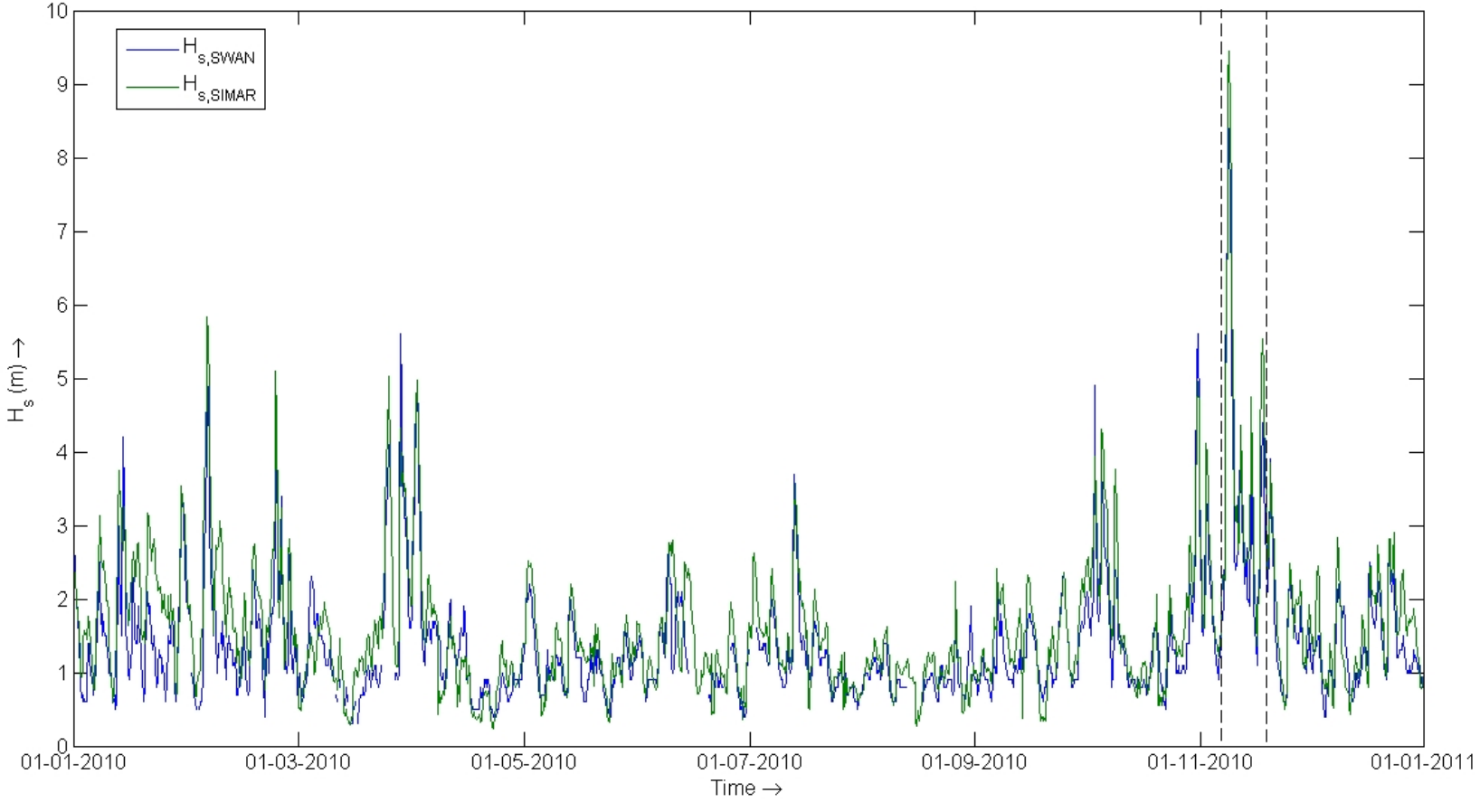
H_s,SWAN
H_s,SIMAR
H_s (m) →
Time →
10
9
8
7
6
5
4
3
2
1
0
01-01-2010
01-03-2010
01-05-2010
01-07-2010
01-09-2010
01-11-2010
01-01-2011

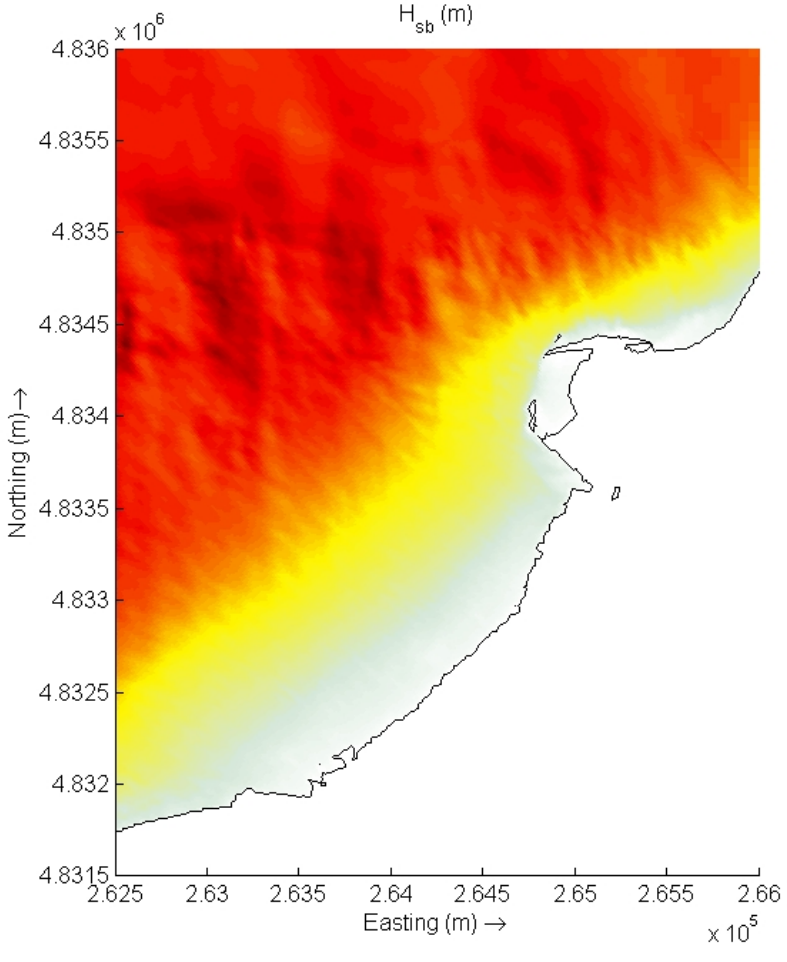
H_{sb} (m)
x 10^6
4.836
4.8355
4.835
4.8345
4.834
4.8335
4.833
4.8325
4.832
4.8315
Northing (m)→
2.625
2.63
2.635
2.64
2.645
2.65
2.655
2.66
Easting (m) →
x 10^5

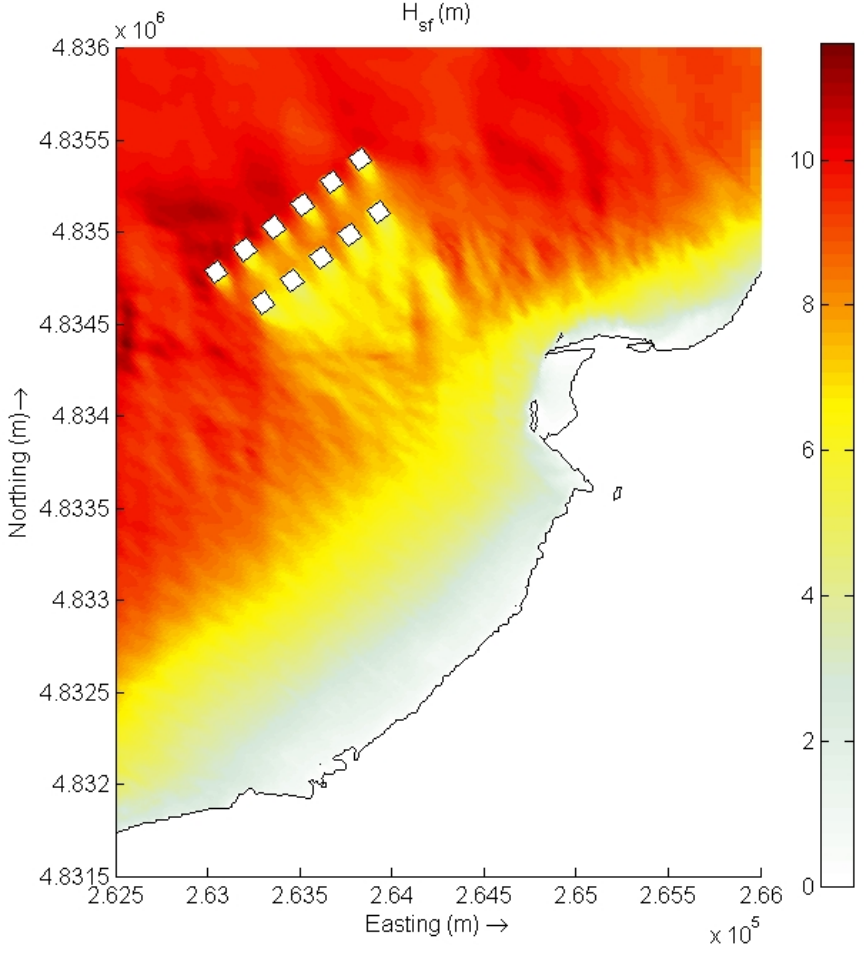
H_{sf} (m)
x 10^6
4.836
4.8355
4.835
4.8345
4.834
4.8335
4.833
4.8325
4.832
4.8315
Northing (m)→
2.625
2.63
2.635
2.64
2.645
2.65
2.655
2.66
Easting (m) →
x 10^5
10
8
6
4
2
0

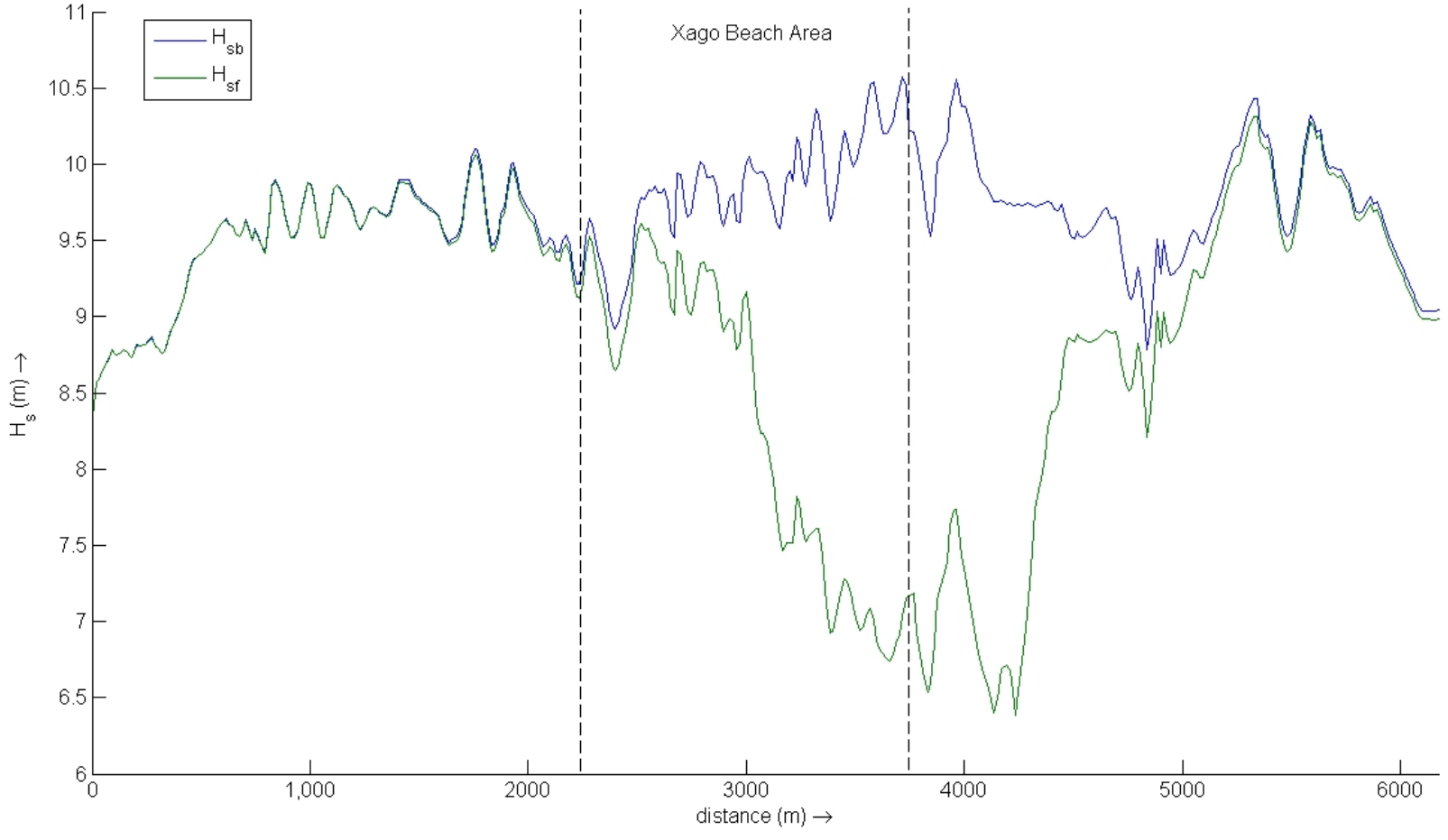
Xago Beach Area
H_{sb}
H_{sf}
H_s (m) →
distance (m) →
11
10.5
10
9.5
9
8.5
8
7.5
7
6.5
6
0
1,000
2000
3000
4000
5000
6000

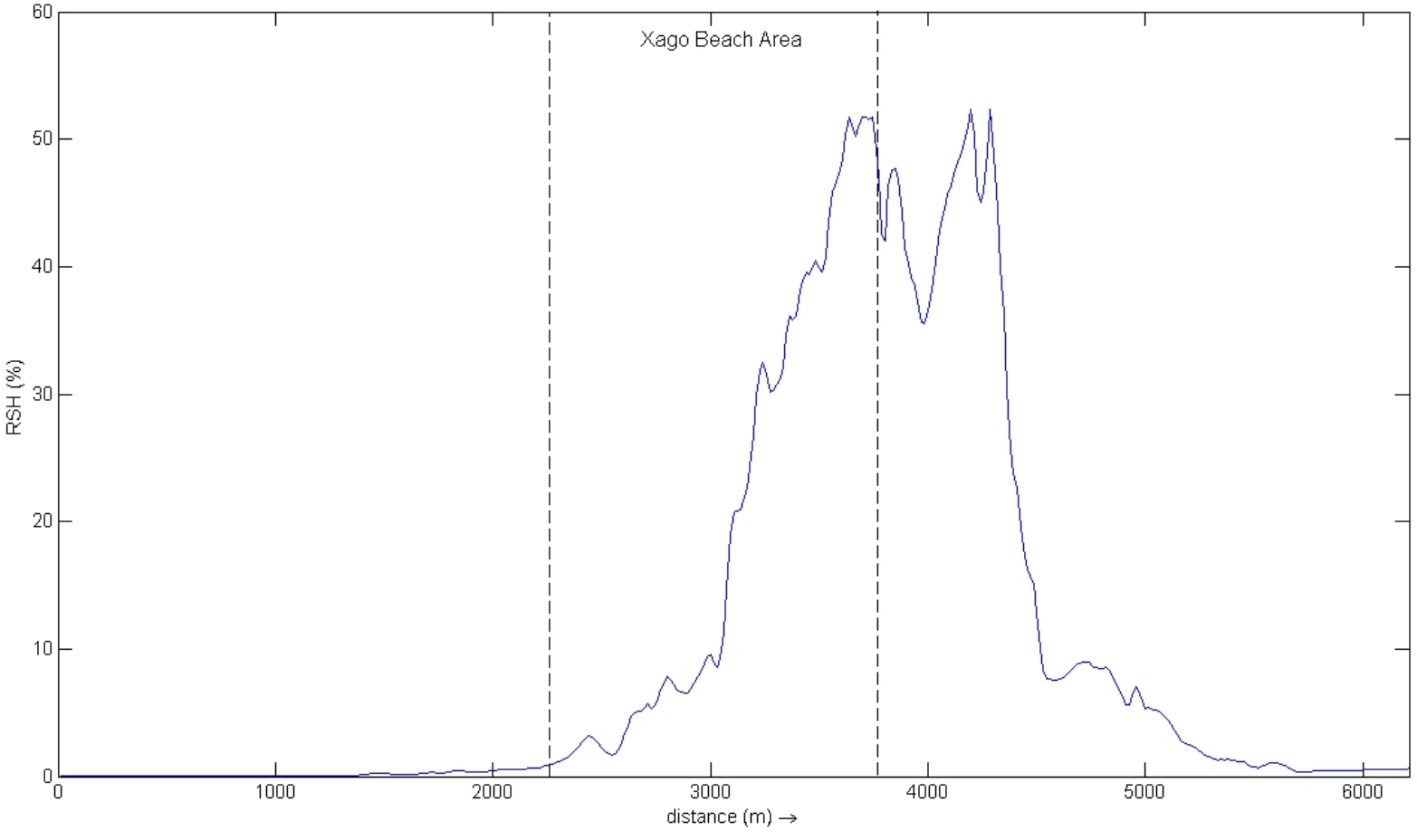
Xago Beach Area
RSH (%)
distance (m) →
0
10
20
30
40
50
60
0
1000
2000
3000
4000
5000
6000

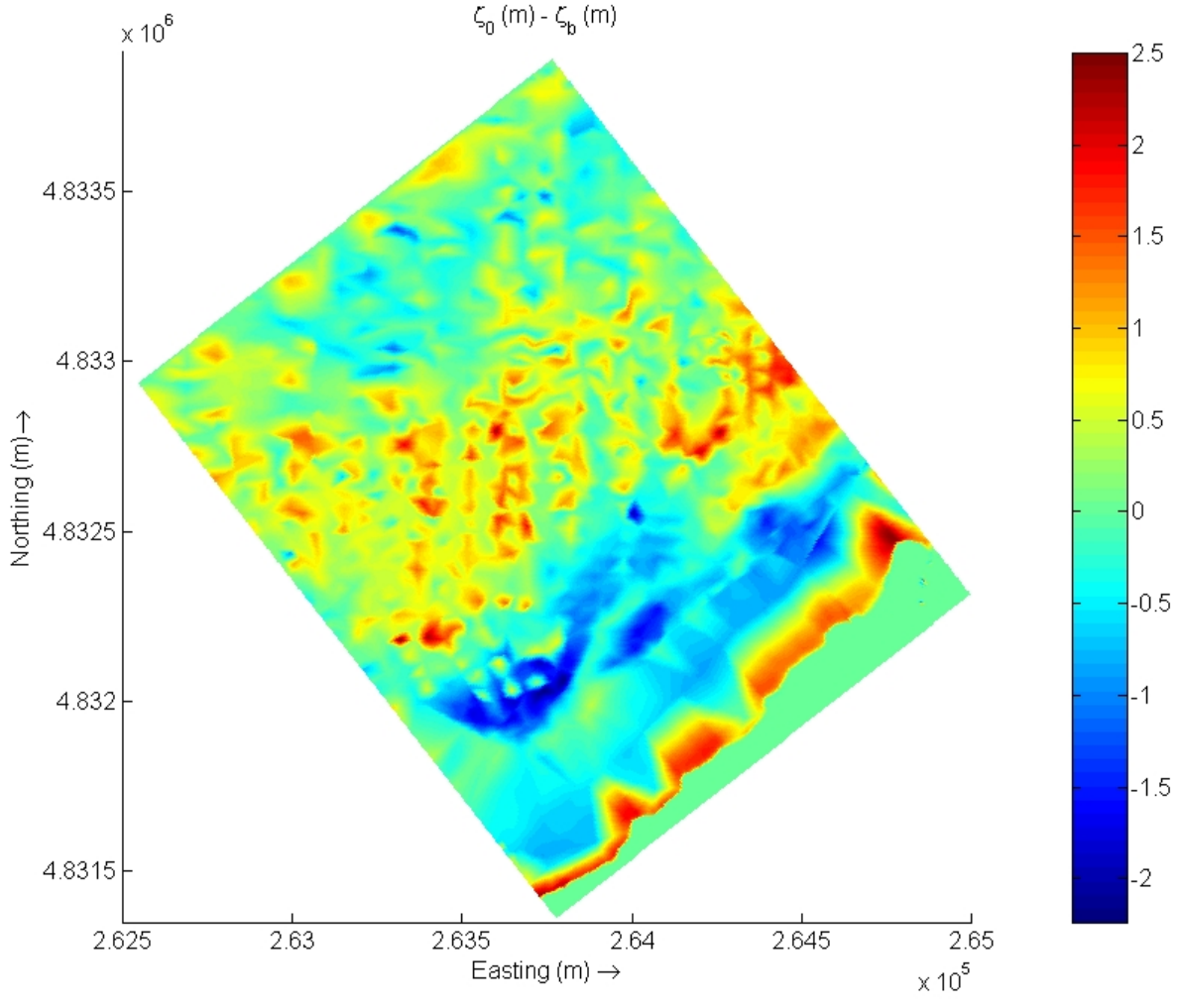
ζ_0 (m) - ζ_b (m)
x 10^6
4.8335
4.833
4.8325
4.832
4.8315
Northing (m) →
2.625
2.63
2.635
2.64
2.645
2.65
Easting (m) →
x 10^5
2.5
2
1.5
1
0.5
0
-0.5
-1
-1.5
-2

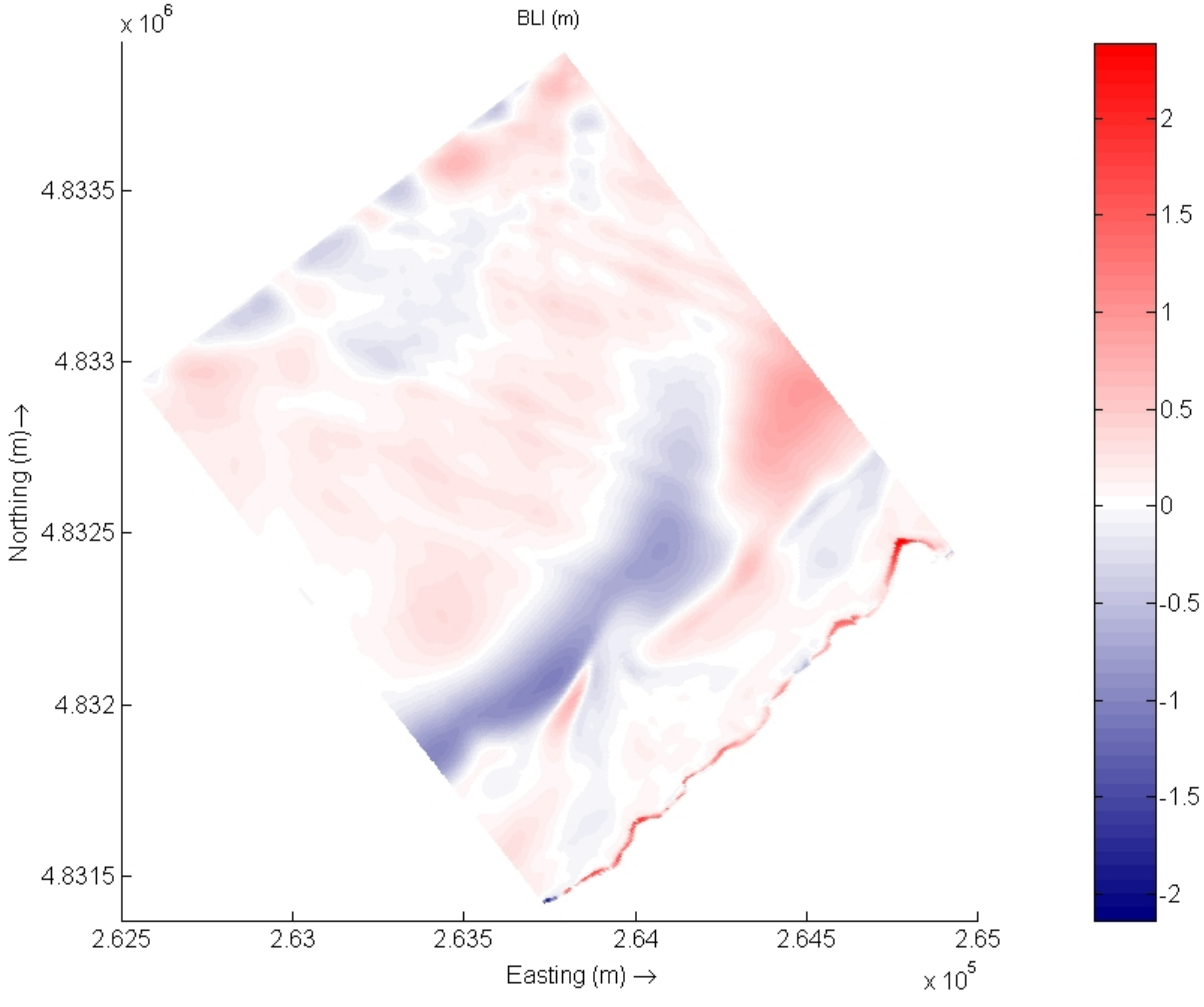
BLI (m)
x 10^6
4.8335
4.833
4.8325
4.832
4.8315
Northing (m) →
2.625
2.63
2.635
2.64
2.645
2.65
Easting (m) →
x 10^5
2
1.5
1
0.5
0
-0.5
-1
-1.5
-2

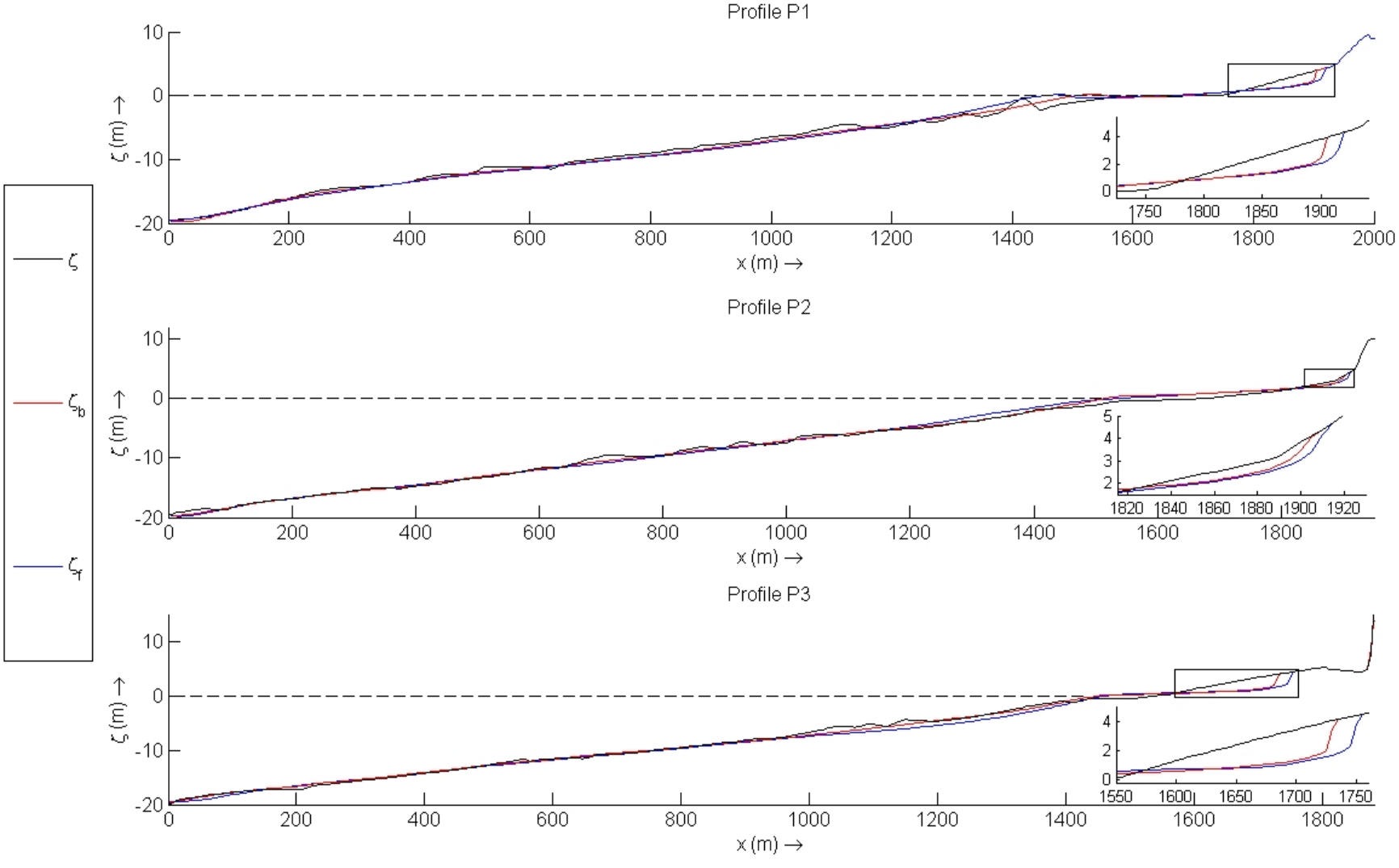
Profile P1
Profile P2
Profile P3
ζ
ζb
ζf
ζ (m) →
x (m) →

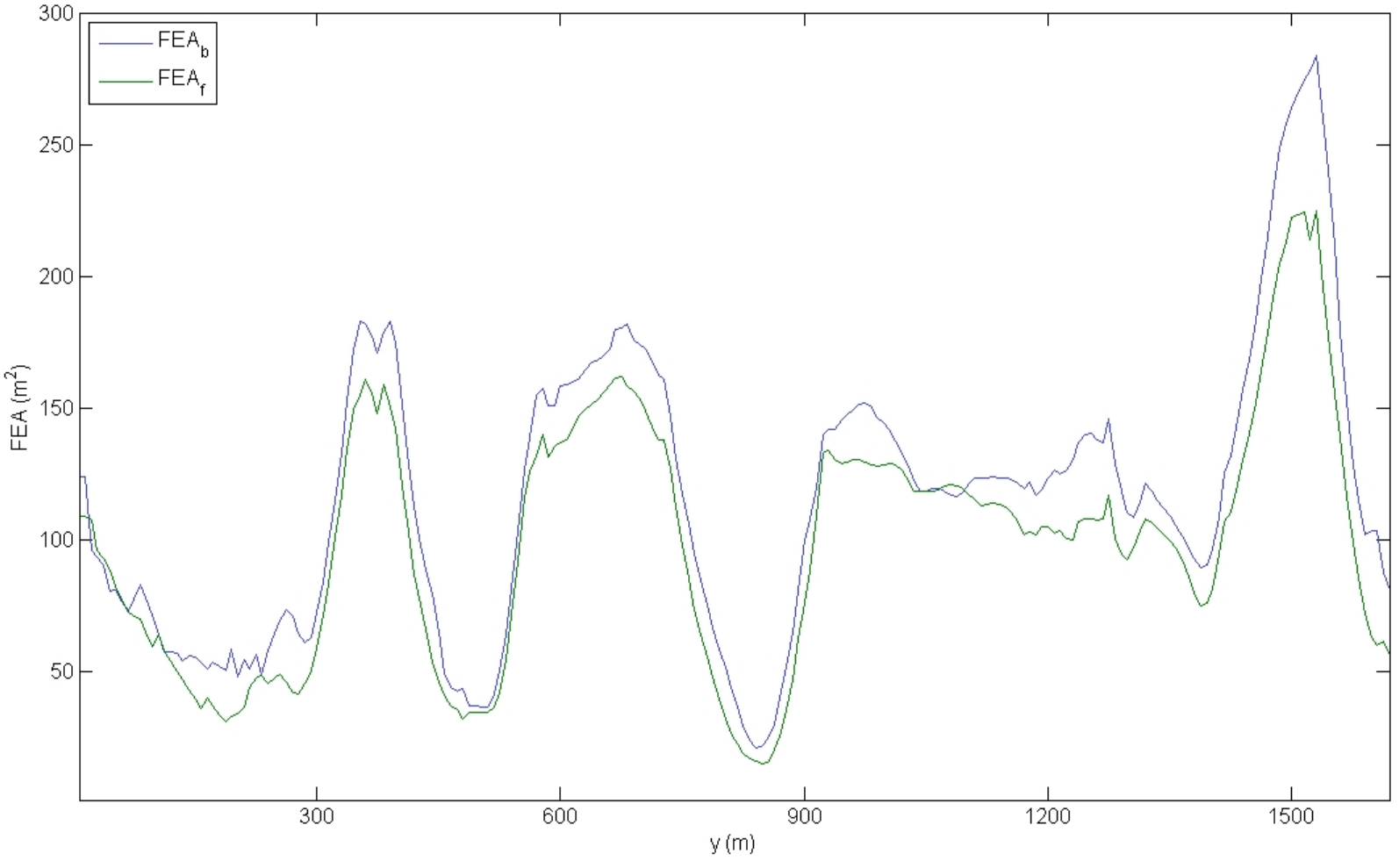
FEA_b
FEA_f
FEA (m^2)
y (m)
300
250
200
150
100
50
300
600
900
1200
1500

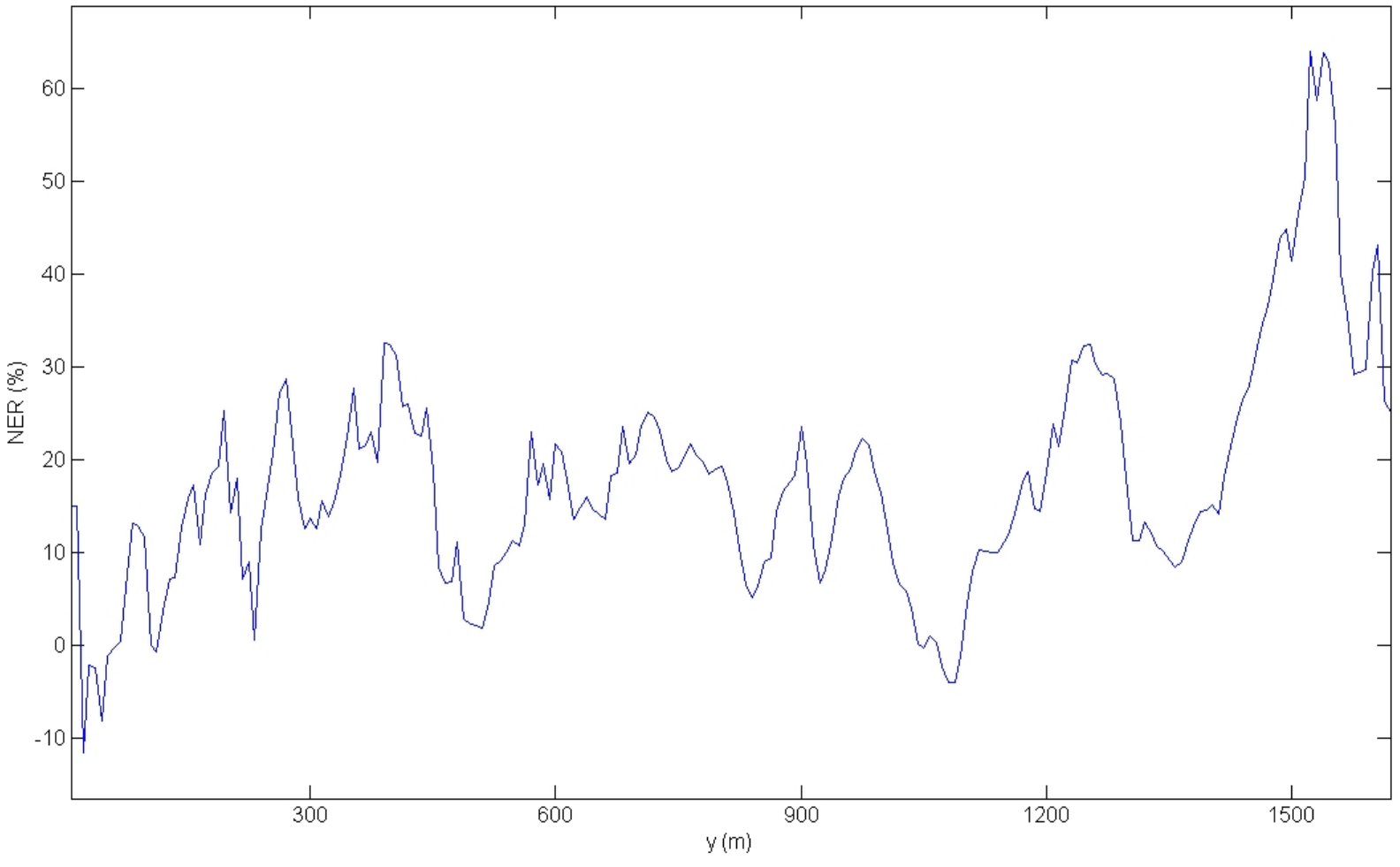
60
50
40
30
20
10
0
-10
NER (%)
300
600
900
1200
1500
y (m)

Data	Data available	Error statistics	
		Root Mean Square Error (*RMSE*) [m]	Coefficient of determination (R^2) [-]
Wave buoy data off Avilés	01/03/2010 – 01/09/2010	0.33	0.89
SIMAR44-3085039 off Xago	01/01/2010 – 01/01/2011	0.45	0.92

Table 1: Wave data used to validate the model and values of the error statistics: Root Mean Square Error (*RMSE*) and coefficient of determination (R^2).